AIAA Guidance, Navigation and Control Conference and Exhibit
18 - 21 August 2008, Honolulu, Hawaii

AIAA 2008-6295

Inertially-Aided Vector Matching Algorithm for Attitude Determination of Spin Stabilized Satellites

Vibhor L. Bageshwar[1], Demoz Gebre-Egziabher[2], William L. Garrard[3]
University of Minnesota, Minneapolis MN 55455

Paul Shestople[4], and Michael Adams[5]
Stanford University, Stanford CA 94305

In this paper, we design and evaluate the performance of two inertially-aided (IA) vector matching algorithm (VMA) architectures for estimating the attitude of a spin stabilized spacecraft. More specifically, we design two attitude determination (AD) systems that use inexpensive commercial-off-the-shelf sensors suitable for application on nanosatellites and evaluate the performance of the resulting AD systems.

For both architectures, the sensor set consists of rate gyros and a three-axis magnetometer (TAM). The stochastic systems are formulated using combinations of attitude dynamic equations, attitude kinematic equations, and sensor measurement models. We evaluate the performance of the IA VMA architectures by using extended Kalman filters to blend post-processed spaceflight data measured on the Stanford Gravity Probe-B spacecraft. We demonstrate that the stochastic systems developed using this sensor set are observable using a series of TAM measurements spanning several epochs. Furthermore, we conduct trade studies to study the effect of rate gyro grade on the errors of the attitude estimates.

Nomenclature

$\vec{b}$ = gyro bias vector
$\vec{b}_0$ = gyro constant null shift vector
$\vec{b}_1$ = gyro bias drift rate vector
$\vec{b}_m$ = magnetometer hard iron bias error vector
C = direction cosine matrix
$C_{a\,b}$ = direction cosine matrix between frame $\mathcal{F}_b$ and frame $\mathcal{F}_a$
C_m = magnetometer misalignment error matrix
C_{MC} = magnetometer calibration matrix
C_{sf} = magnetometer scale factor error matrix
C_{si} = magnetometer soft iron error matrix
$\hat{e}$ = Euler axis unit vector
$\vec{G}_{ext}$ = external torque vector
F = continuous-time state error mapping matrix
$\vec{h}$ = angular momentum vector
H = measurement matrix
I = moment of inertia, principal axis frame
J = performance index, Wahba's problem
$\vec{m}$ = model, Earth magnetic field vector
$\vec{m}_m$ = measured, Earth magnetic field vector
$\vec{n}_b$ = gyro bias, driving process noise
$\vec{n}_g$ = gyro additive wide band measurement noise vector
$\vec{n}_m$ = magnetometer additive wide band measurement noise vector
$\mathcal{O}$ = observability matrix
p, q = quaternion
P = discrete-time state covariance matrix

[1] Dept. of Aerospace Eng. and Mechanics; currently at Honeywell International, Golden Valley, MN, Member AIAA
[2] Assistant Professor, Dept. of Aerospace Eng. and Mechanics, Member AIAA
[3] Professor and Director of the Minnesota Space Grant Consortium, Dept. of Aerospace Eng. and Mechanics, Fellow AIAA
[4] Gravity Probe B, Hansen Experimental Physics Laboratory; currently at Space Systems/Loral, Palo Alto, CA, Member AIAA
[5] Gravity Probe B, Hansen Experimental Physics Laboratory

Q = discrete-time process noise covariance matrix
Q_{b1} = power spectral density, gyro driving process noise
Q_W = power spectral density matrix, process noise vector
R = measurement noise covariance matrix
$\vec{u}$ = general vector
$\mathcal{U}$ = set of arbitrary vectors, $\vec{u}_i$
$\vec{v}$ = measurement noise vector
$\vec{w}$ = process noise vector
$\vec{x}$ = state vector
$\vec{z}$ = measurement vector

$\mathcal{F}_b$ = body frame
$\mathcal{F}_{\hat{b}}$ = estimated body frame
$\mathcal{F}_g$ = gyro body frame
$\mathcal{F}_N$ = navigation frame
$\mathcal{F}_{\hat{N}}$ = estimated navigation frame

$\alpha, \beta, \gamma, \kappa$ = tuning parameters
δ = Dirac delta function
Γ = discrete-time process noise mapping matrix
Γ_c = continuous-time process noise mapping matrix
$\vec{\omega}$ = angular velocity vector
$\vec{\omega}_m$ = measured angular velocity vector
$\Omega(\cdot)$ = left quaternion operator
ϕ = rotation angle about Euler axis unit vector
Φ = discrete-time state error mapping matrix
σ_b = standard deviation, gyro bias driving process noise
σ_{b1} = standard deviation, gyro bias drift rate
σ_g = standard deviation, gyro measurement noise
τ = correlation time, gyro bias drift rate

$(\cdot)_1$ = inertially-aided vector matching algorithm architecture 1
$(\cdot)_2$ = inertially-aided vector matching algorithm architecture 2
$(\cdot)_b$ = body frame
$(\cdot)_N$ = navigation frame
$(\cdot)_g$ = gyro or gyro sensor frame
$\hat{(\cdot)}$ = estimated value of $(\cdot)$
$(\cdot)^\times$ = skew symmetric operator
$E\{(\cdot)\}$ = expected value of $(\cdot)$

$\delta\vec{b}$ = gyro bias error vector
$\delta\vec{G}_{ext}$ = external torque error vector
$\delta\vec{h}$ = angular momentum error vector
δI = modeling error, moment of inertia, principal axis frame
δq = quaternion error
δq_b = quaternion error from true body frame to estimated body frame
δq_N = quaternion error from true navigation frame to estimated navigation frame
$\delta\vec{x}$ = state error vector
$\delta\vec{z}$ = measurement error vector

I. Introduction

Attitude refers to a vehicle's angular orientation in space. The attitude of a vehicle can be defined by specifying the relative orientation of two reference frames. For spacecraft guidance, navigation, and control applications in Earth orbit, the two reference frames typically used are a vehicle fixed body frame and a navigation frame with known orientation. The navigation frame generally refers to an inertial frame, an Earth fixed frame, or a local vertical local horizontal frame. The selection of a navigation frame depends on the application. Attitude

determination (AD) systems are used to estimate the orientation of a vehicle or, more specifically, to estimate the orientation of the body frame relative to the navigation frame.

In general, an AD system consists of a set of sensors to measure the vehicle's attitude; a stochastic system consisting of a dynamic model, measurement model, and sensor measurement models; and a filter that blends the sensor measurements to compute estimates of the vehicle's attitude. The selection of an attitude sensor depends on its physical dimensions, operating characteristics, and performance characteristics. The attitude sensors typically used for spacecraft AD systems include inertial sensors, star trackers, Sun sensors, horizon sensors, and three-axis magnetometers (TAMs). These sensors have been used to mechanize highly accurate AD systems, however, they may not be suitable for some emerging applications. Nanosatellites, for example, are a class of small satellites that have restrictions on size, mass, and available power. An AD system designed for a nanosatellite is subject to these restrictions which limit the selection and number of onboard attitude sensors that can be used for nanosatellite AD systems. Furthermore, certain nanosatellites, such as the one discussed in [1], are designed using inexpensive, commercial off-the-shelf (COTS) components.

The scientific missions of these nanosatellites often require real time AD systems. These nanosatellites are often not passively stabilized but are equipped with control actuators that enable low bandwidth attitude maneuvers. One sensor set that satisfies the various constraints of a nanosatellite includes an orthogonal triad of rate gyros and a TAM. In this paper, we describe the design of an AD system that uses an extended Kalman filter (EKF) to blend measurements from rate gyros and a TAM to estimate a spin stabilized spacecraft's attitude in three axes. The measurement model of the stochastic system is designed using a vector matching approach.

A. Vector Matching

Vector matching using multiple reference frames is referred to as Wahba's problem [2]. The objective of Wahba's problem is to compute a least squares estimate of the direction cosine matrix (DCM) between a vehicle's navigation and body frames. If we define a navigation frame, $\mathcal{F}_N$, and a body frame, $\mathcal{F}_b$, with common origin, then Wahba's problem can be stated as follows:

Given a set of vectors, $\bar{u}_1^b$, $\bar{u}_2^b$, ..., $\bar{u}_n^b$, $\forall\ n \geq 2$, measured in $\mathcal{F}_b$ and the same set of vectors known in $\mathcal{F}_N$, $\bar{u}_1^N$, $\bar{u}_2^N$, ... $\bar{u}_n^N$, compute the DCM that minimizes the performance index

$$J = \sum_{i=2}^{n} \|\bar{u}_i^b - C_{b\,N}(q)\bar{u}_i^N\|^2 \tag{1}$$

subject to the attitude quaternion unit constraint

$$q \cdot q = ||q||^2 = q_1^2 + q_2^2 + q_3^2 + q_4^2 = 1 \tag{2}$$

where $C_{b\,N}$ refers to the DCM between $\mathcal{F}_N$ and $\mathcal{F}_b$. The superscript following a matrix indicates that the scalar components of the corresponding vector are expressed with respect to the basis vectors of the indicated reference frame.

In this approach, the attitude of a vehicle is estimated by matching at least two vectors that are measured in $\mathcal{F}_b$ to the same set of vectors that are known, or modeled, in $\mathcal{F}_N$. The vectors are matched by computing the DCM that minimizes the difference between the scalar components of the measured vectors and the scalar components of the modeled vectors resolved in $\mathcal{F}_b$. A unique solution to Wahba's problem requires at least two non-zero, non-collinear vectors because at least two vectors are required to uniquely define a plane. Therefore, if only one unique vector measurement is available, then Wahba's problem does not have a unique solution because there is a rotational ambiguity about the axis aligned with the vector measurement.

There are four general categories of algorithms that have been developed to estimate the attitude of a vehicle using vector matching. The first category consists of analytic solutions to Wahba's problem [3], [4]. The second category consists of algorithms that directly solve the least squares optimization problem using a batch [5] or recursive process [6]. These algorithms use optimal solutions to Wahba's problem to estimate attitude that directly preserve the problem constraints. However, these algorithms do not incorporate a dynamic model or sensor, such as a rate gyro, measurement models into their formulation. The third category consists of filtering algorithms that solve Wahba's problem such as an Euler angle filter [7], DCM filter [8], Rodrigues parameter filter [9], and quaternion filters [10], [11]. The application of a filter enables a dynamic model and sensor measurement models to be incorporated into the algorithm. However, the attitude estimates are sub-optimal. The filter

uses linearized versions of nonlinear models in its formulation and, thus, the filter based solutions are unable to directly preserve the problem constraints. The fourth category consists of filtering algorithms that solve the least squares optimization problem and directly preserve the problem constraints [12].

B. Objectives and Methodology of Current Work

In the AD system designed in this paper, the attitude of the spacecraft is measured by rate gyros, or simply gyros, and a TAM. Gyros are high bandwidth sensors and measure the spacecraft's angular velocity vector. Integrating these measurements once yields the spacecraft's attitude. However, gyro measurements are corrupted by errors such as slowly time-varying biases and wide band noise. Integrating these measurement errors result in potentially unbounded errors in the gyro based estimates of the spacecraft's attitude. These attitude errors can be bounded using measurements from aiding sensors such as the TAM. TAMs are typically low bandwidth sensors that measure the vehicle's attitude independently of the gyros. The measurements from aiding sensors can be used to periodically estimate the gyro biases and reset the gyro based estimates of the spacecraft's attitude, Fig. 1.

In general, to estimate the gyro biases and reset the gyro based estimate of the spacecraft's attitude, the aiding system sensors must provide three axis measurements of attitude without rotational ambiguity along any axis at a single epoch. The attitude of a spacecraft is unobservable using a TAM measurement at a single epoch because there is a rotational ambiguity about the axis aligned with the local Earth magnetic field (EMF) vector. Therefore, a TAM measurement at a single epoch does not contain sufficient information to estimate the gyro biases and reset the gyro based estimates of the spacecraft's attitude. However, if the direction of the local EMF vector varies relative to the spacecraft as the spacecraft orbits the Earth, then the direction of the vector measurements from the TAM varies over a series of epochs. In this case, the attitude of a spacecraft could become observable when using a set of TAM measurements spanning a series of epochs.

A TAM provides three axis measurements of attitude over a series of epochs only if the spacecraft's inclination angle or angular velocity allows the direction of the local EMF vector to vary significantly as the spacecraft orbits the Earth. This set of measurements may contain sufficient information to estimate the gyro biases and reset the gyro based estimates of the spacecraft's attitude. However, if the integrated errors of the gyro bias become large and the direction of the local EMF vector has not varied significantly over a set of TAM measurements, then these TAM measurements may not be sufficient to estimate the gyro bias and reset the gyro based estimates of the spacecraft's attitude.

There are two potential approaches that can be used to assist the aiding sensor and reset the gyro based estimate of the spacecraft's attitude. The first approach is to select a gyro that has a small, stable bias. This approach constrains the magnitude of the gyro bias before it is integrated to limit the effect of the bias on the gyro based estimates of the spacecraft's attitude. The second approach is to mathematically constrain the gyro based estimates of the spacecraft's attitude. This approach uses the attitude dynamics of the spacecraft to limit the magnitude of the errors in the gyro based estimates of the spacecraft's attitude after the gyro bias has been integrated.

This paper has three main objectives. The first objective is to design two inertially aided (IA) vector matching algorithm (VMA) architectures for spacecraft AD systems. The VMA [13] is a filtering algorithm used to numerically solve Wahba's problem and estimate the attitude of a vehicle. In the VMA, a measurement model is derived from the linearization of the DCM between the vehicle's body and navigation frames. The model can incorporate any number of vector measurements at a single epoch. The VMA is then extended by incorporating two vehicle dynamic models based on a quaternion parameterization of attitude. The first model includes the vehicle's attitude kinematic equations and a gyro measurement model. The second model includes the vehicle's attitude dynamic equations, vehicle's attitude kinematic equations, and a gyro measurement model. We will refer to the stochastic system corresponding to these models as IA VMA architectures.

The second objective is to implement an EKF to blend measurements from the gyros and aiding sensor for both IA VMA architectures using spaceflight data. The third objective is to conduct trade studies to evaluate the EKF performance as a function of the IA VMA architecture and quality of gyro, or gyro grade. The performance analysis is conducted using Monte Carlo simulations and an analysis of the resulting statistics of the estimated state vector for both architectures. The trade studies are used to determine the effect of gyro grade on the performance of both architectures, to determine the effect of including constraints on the vehicle's attitude motion on the performance of both architectures, and to determine the feasibility of using this particular set of sensors for spacecraft AD systems.

This paper is organized as follows. In Section II, we develop the dynamic models for both IA VMA architectures. In Section II, we derive the linearized measurement model for both IA VMA architectures. In Section IV,

we summarize the EKF algorithm implemented for both IA VMA architectures. In Section V, we evaluate the performance of the IA VMA architectures using post-processed spaceflight data.

II. Dynamic Models

The dynamic models for both IA VMA architectures are formulated using attitude dynamic equations, attitude kinematic equations, and a gyro measurement model. This section describes the formulation of the state vector equations, the linearized state vector equations, and the state error covariance matrix equations for both architectures.

A Rate Gyro Measurement Model

Rate gyros measure the angular velocity of the vehicle to which they are affixed. However, the gyro measurements are corrupted by errors caused by characteristics of the gyros and the environment in which the gyros operate. The gyro measurement errors include both correlated and uncorrelated components. Therefore, a gyro measurement model must incorporate both types of error components to relate the measured angular velocity to the true angular velocity of the vehicle [14]. A typical gyro measurement model [14] is

$$C_{b\,g}\bar{\omega}^g_m(t) = \bar{\omega}^b(t) + C_{b\,g}(\bar{b}^g(t) + \bar{n}^g_g(t)) \tag{3}$$

where $\vec{\omega}$ refers to the true angular velocity vector, $\vec{\omega}_m$ refers to the measured angular velocity vector, $\vec{b}$ refers to the gyro bias vector, and $\vec{n}_g$ refers to additive wide band measurement noise vector. The matrix $C_{b\,g}$ refers to the DCM between the gyro sensor frame and the vehicle's body frame. If these two reference frames are aligned, then $C_{b\,g}$ is the identity matrix.

A model for a time-varying gyro bias [14] is

$$\bar{b}^g(t) = \bar{b}^g_0 + \bar{b}^g_1(t) \tag{4}$$

where $\vec{b}_0$ refers to a constant null shift vector and $\vec{b}_1$ refers to a time-varying bias vector, or bias drift rate. The bias drift rate can be modeled as a zero-mean, Gaussian, exponentially correlated process. For a single gyro,

$$\dot{b}^g(t) = \dot{b}^g_1(t) = -\frac{1}{\tau}b^g_1(t) + n^g_b(t) \tag{5a}$$

$$E\{b^g_1(t)\} = 0 \tag{5b}$$

$$E\{b^g_1(t)b^g_1(\tau)\} = \sigma^2_{b1}\exp[-t/\tau] \tag{5c}$$

$$Q_{b1} = \frac{2\sigma^2_{b1}}{\tau} \tag{5d}$$

where σ_{b1} refers to the standard deviation of the process b_1, τ refers to the correlation time of the process b_1, $\vec{n}_b$ refers to the driving process noise, Q_{b1} refers to the power spectral density of $\vec{n}_b$, and $\delta(t-\tau)$ denotes the Dirac delta function. The vector $\vec{n}_b$ can be modeled as a zero-mean, Gaussian, white noise process or sequence. For a single gyro,

$$E\{n^g_b(t)\} = 0 \tag{6a}$$

$$E\{n^g_b(t)n^g_b(\tau)\} = \sigma^2_b\delta(t-\tau) \tag{6b}$$

where σ_b refers to the standard deviation of the driving process noise.

The additive, wide band gyro measurement noise is normally referred to as output noise on gyro specification sheets [14]. This noise can be modeled as a zero-mean, Gaussian, white noise process or sequence. For a single gyro

$$E\{n^g_g(t)\} = 0 \tag{7a}$$

$$E\{n^g_g(t)n^g_g(\tau)\} = \sigma^2_g\delta(t-\tau) \tag{7b}$$

where σ_g refers to the standard deviation of the gyro measurement noise. It should be noted that the measurement noise has a higher frequency content than the bias drift rate.

The relationship between the measured and estimated angular velocity can be determined by taking the expected value of Eq. (3)

$$E\{C_{b\,g}\bar{\omega}_m^g(t)\} = E\{\bar{\omega}^b(t)\} + E\{C_{b\,g}\bar{b}^g(t)\} + E\{C_{b\,g}\bar{n}_g^g(t)\}$$
$$\hat{\bar{\omega}}^b(t) = C_{b\,g}\bar{\omega}_m^g(t) - C_{b\,g}\hat{\bar{b}}^g(t) \tag{8}$$

where $\hat{\bar{\omega}}$ refers to the mean of the estimated angular velocity vector and $\hat{\vec{b}}$ refers to the mean of the estimated gyro bias vector. A given measurement is deterministic and, thus, the expected value of a measurement is simply the measurement itself. If Eq. (3) is substituted into Eq. (8), then the difference between the true and estimated angular velocity can be written as

$$\bar{\omega}^b(t) - \hat{\bar{\omega}}^b(t) = -C_{b\,g}[\bar{b}^g(t) - \hat{\bar{b}}^g(t) + \bar{n}_g^g(t)] \tag{9}$$

If we define the gyro bias error vector, $\delta\vec{b}$, to be the difference between the true and estimated gyro bias vectors

$$\delta\bar{b}^g(t) = \bar{b}^g(t) - \hat{\bar{b}}^g(t) = \bar{b}_1^g(t) \tag{10}$$

then Eq. (9) can be rewritten as

$$\bar{\omega}^b(t) - \hat{\bar{\omega}}^b(t) = -C_{b\,g}[\delta\bar{b}^g(t) + \bar{n}_g^g(t)] \tag{11}$$

The differential equation of the estimated gyro bias can be determined by taking the expected value of Eq. (5a)

$$E\left\{\frac{d}{dt}\bar{b}^g(t)\right\} = E\left\{-\frac{1}{\tau}\bar{b}_1^g(t)\right\} + E\{\bar{n}_b^g(t)\}$$
$$\frac{d}{dt}\hat{\bar{b}}^g(t) = \bar{0} \tag{12}$$

where it has been assumed that the differential and expectation operators can be interchanged. The differential equation of the gyro bias error can be determined by differentiating Eq. (10) and substituting Eqs. (5a) and (12) into the resulting equation

$$\dot{\delta\bar{b}}^g(t) = \frac{d}{dt}\bar{b}^g(t) - \frac{d}{dt}\hat{\bar{b}}^g(t) = -\frac{1}{\tau}\delta\bar{b}^g(t) + \bar{n}_b^g(t) \tag{13}$$

B. Attitude Kinematic Equations

Attitude kinematic equations are first-order differential equations that relate angular velocity to attitude rates. These equations can be used to compute estimates of a vehicle's attitude from measurements of the vehicle's angular velocity. The formulation of the attitude kinematic equations depends on the attitude parameterization. The attitude kinematic equations are functions of both the vehicle's angular velocity and current attitude regardless of the attitude parameterization.

Two commonly used attitude parameterizations are Euler angles and quaternions. Attitude kinematic equations formulated using Euler angles have a singularity when computing Euler angle rates from angular velocity. A singularity occurs for every three component sequence of Euler angles. Therefore, Euler angles can be used to parameterize attitude only in applications where the vehicle's attitude does not approach the singular orientation for the selected three component sequence. In this paper, quaternions are used to parameterize the vehicle's attitude.

A quaternion consists of four scalar components, three of which refer to a vector component [15]. Quaternions use four components to parameterize a three dimensional orientation and, thus, only three of the four components are independent. A quaternion can be defined as

$$q = [\, q_1 \quad q_2 \quad q_3 \quad q_4 \,]^T = \begin{bmatrix} \bar{q} \\ q_4 \end{bmatrix} \tag{14}$$

subject to the quaternion unit constraint, Eq. (2), where q_1, q_2, and q_3 comprise the quaternion vector component and q_4 comprises the quaternion scalar component. We define the left quaternion operator to simplify notation in the following sections

$$\Omega(q) = \begin{bmatrix} q_4\bar{1}_3 - \bar{q}^\times & \bar{q} \\ -\bar{q}^T & q_4 \end{bmatrix} \tag{15}$$

A rotation from one reference frame to a second reference frame, parameterized by the quaternion q, followed by a rotation from the second reference frame to a third reference frame, parameterized by the quaternion p, can be written as the quaternion product

$$C(p)C(q) = C(p \otimes q) \tag{16}$$

The convention used in this paper is that the quaternions are multiplied in the same order as suggested by the multiplication of DCMs.

If a small angle assumption (SAA) is made to describe the orientation of one reference frame relative to a second reference frame, then the DCM between these two reference frames differs from the identity matrix infinitesimally. If the small angle assumption is applied a quaternion, then

$$\bar{q} = \delta\bar{q} \tag{17a}$$

$$q_4 \sim 1 \tag{17b}$$

The DCM formulated using quaternions under the small angle assumption can be written as

$$C_{SAA} \sim \bar{1}_3 - 2\delta\bar{q}^\times \tag{18}$$

where the second order term $\delta\bar{q}\delta\bar{q}^T \sim \bar{0}$.

The attitude kinematic equations [15] are

$$\dot{q}(t) = \frac{1}{2}\begin{bmatrix} -\bar{\omega}^{b\times}(t) & \bar{\omega}^b(t) \\ -\bar{\omega}^{bT}(t) & 0 \end{bmatrix} q(t) = \frac{1}{2}\Omega\begin{bmatrix} \bar{\omega}^b(t) \\ 0 \end{bmatrix} q(t) \tag{19}$$

These equations have no singularities and, thus, quaternion rates can be computed from angular velocity for any orientation of the vehicle. Furthermore, these equations are not functions of transcendental functions as would be the case if these equations were formulated using Euler angle parameterizations. However, transcendental functions and their effect on the required on-board computational power will not be addressed here.

C. Attitude Kinematic Error Equations

The attitude of a vehicle is defined by specifying the orientation of the vehicle's body frame relative to the vehicle's navigation frame. The relative orientation of the two reference frames is specified using a DCM parameterized by quaternions. The EKF computes estimates of the quaternions used to parameterize this DCM and, thus, the orientation of the body frame relative to the navigation frame. The body frame computed from a DCM formulated using the estimated quaternions will be referred to as the estimated body frame, $\mathcal{F}_{\hat{b}}$.

The relationship between the true quaternion, q, and the estimated quaternion, $\hat{q}$, [16] is

$$q(t) = \delta q(t) \otimes \hat{q}(t) \tag{20}$$

Equation (20) suggests that the rotation from the navigation frame to the body frame, parameterized by q, is equal to the rotation from the navigation frame to the estimated body frame, parameterized by $\hat{q}$, followed by a rotation from the estimated body frame to the body frame, parameterized by δq. δq refers to the quaternion estimation error and represents the orientation error between the actual and estimated body frames. We will assume that δq refers to a small angle rotation about the estimated body frame.

The attitude kinematic equations for the true and estimated quaternions can be written using Eq. (19)

$$\dot{q} = \frac{1}{2}\begin{bmatrix} \bar{\omega}^b \\ 0 \end{bmatrix} \otimes q = \frac{1}{2}\begin{bmatrix} \bar{\omega}^b \\ 0 \end{bmatrix} \otimes (\delta q \otimes \hat{q}) \tag{21a}$$

$$\dot{\hat{q}} = \frac{1}{2}\begin{bmatrix} \hat{\bar{\omega}}^b \\ 0 \end{bmatrix} \otimes \hat{q} \tag{21b}$$

where Eq. (20) has been substituted into Eq. (21a). The differential equation for the quaternion estimation error [16] is

$$\delta\dot{q} = \frac{1}{2}\begin{bmatrix}\bar{\omega}^b - \hat{\bar{\omega}}^b \\ 0\end{bmatrix} \otimes \delta q - \begin{bmatrix}\hat{\bar{\omega}}^{b\times}\delta\bar{q} \\ 0\end{bmatrix} \tag{22}$$

where Eq. (22) has been derived without appealing to any assumptions. If we now appeal to the small angle assumption when considering $\delta\dot{q}$, then $\delta\dot{q}$ can be written as

$$\delta\dot{q} = \frac{d}{dt}\begin{bmatrix}\delta\bar{q} \\ 1\end{bmatrix} = \frac{1}{2}\begin{bmatrix}-(\bar{\omega}^b - \hat{\bar{\omega}}^b)^\times & \bar{\omega}^b - \hat{\bar{\omega}}^b \\ -(\bar{\omega}^b - \hat{\bar{\omega}}^b)^T & 0\end{bmatrix}\begin{bmatrix}\delta\bar{q} \\ 1\end{bmatrix} - \begin{bmatrix}\hat{\bar{\omega}}^{b\times}\delta\bar{q} \\ 0\end{bmatrix} \tag{23}$$

There are two dynamic models used in the design of the IA VMA architectures. The first model does not include the vehicle's attitude dynamics whereas the second model does include the vehicle's attitude dynamics. Therefore, the expressions for $\delta\dot{\bar{q}}$ will be derived to incorporate angular momentum for the second model. This extra term is included in the model to ensure the linearized stochastic system for the second IA VMA architecture is deterministically observable.

For the first dynamic model, if Eq. (11) is substituted into Eq. (23), then $\delta\dot{\bar{q}}$ can be rewritten as

$$\begin{aligned}\delta\dot{\bar{q}}(t) &= -\hat{\bar{\omega}}^{b\times}\delta\bar{q} - \frac{1}{2}(C_{b\,g}[\delta\bar{b}^g + \bar{n}_g^g]) + \frac{1}{2}(C_{b\,g}[\delta\bar{b}^g + \bar{n}_g^g])^\times\delta\bar{q} \\ &\sim -\hat{\bar{\omega}}^{b\times}(t)\delta\bar{q}(t) - \frac{1}{2}C_{b\,g}\delta\bar{b}^g(t) - \frac{1}{2}C_{b\,g}\bar{n}_g^g(t)\end{aligned} \tag{24}$$

where the second order error terms are assumed to be very small.

For the second dynamic model, the second order error terms of Eq. (24) will be rewritten using the angular momentum of the vehicle. The true and estimated angular momentum of the vehicle can be written as

$$\bar{h}^b(t) = I\bar{\omega}^b(t) \tag{25a}$$

$$\hat{\bar{h}}^b(t) = (I + \delta I)\,\hat{\bar{\omega}}^b(t) \tag{25b}$$

where the vehicle's body frame is assumed to be a principal axis frame. I refers to the moment of inertia of the vehicle written in a principal axis frame and δI refers to modeling errors in the moment of inertia. Using Eq. (25), $\bar{\omega}^b - \hat{\bar{\omega}}^b$ can be written as

$$\bar{\omega}^b - \hat{\bar{\omega}}^b = I^{-1}(\bar{h}^b - \hat{\bar{h}}^b) + I^{-1}\delta I\hat{\bar{\omega}}^b \tag{26}$$

If Eqs. (11) and (26) are substituted into Eq. (23), then $\delta\dot{\bar{q}}$ can be rewritten as

$$\begin{aligned}\delta\dot{\bar{q}}(t) &= -\hat{\bar{\omega}}^{b\times}\delta\bar{q} - \frac{1}{2}(C_{b\,g}[\delta\bar{b}^g + \bar{n}_g^g]) - \frac{1}{2}(I^{-1}\delta\bar{h}^b + I^{-1}\delta I\hat{\bar{\omega}}^b)^\times\delta\bar{q} \\ &= -\hat{\bar{\omega}}^{b\times}(t)\delta\bar{q}(t) - \frac{1}{2}C_{b\,g}\delta\bar{b}^g(t) - \frac{1}{2}C_{b\,g}\bar{n}_g^g(t) + \frac{1}{2}\delta\bar{q}^\times(t)I^{-1}\delta\bar{h}^b(t) - \frac{1}{2}(I^{-1}\delta I\hat{\bar{\omega}}^b(t))^\times\delta\bar{q}(t)\end{aligned} \tag{27}$$

D. Attitude Dynamic Equations

The attitude dynamics of a vehicle can be described using Euler's equations [17]. Euler equations written in a principal axis frame are

$$\dot{\bar{h}}^b(t) = -\bar{\omega}^{b\times}(t)\bar{h}^b(t) + \bar{G}_{ext}^b(t) \tag{28}$$

where $\vec{G}_{ext}$ refers to the external torque vector acting on the rigid body and includes control torques and environmental disturbance torques. These environmental disturbance torques depend on the vehicle's operating environment. For spacecraft operating in LEO, the environmental disturbance torques include gravity gradient torques, aerodynamic torques, magnetic torques, and solar radiation torques. It should be noted that the magnitude of these torques is altitude dependent.

E. Attitude Dynamic Error Equations

The angular momentum of a vehicle is computed by propagating Euler's equations using the vehicle's angular velocity, control torques, and environmental disturbance torques. The EKF propagates Euler's equations using

measurements of angular velocity corrected by the posterior estimate of the gyro bias, models or measurements of the control torques, and models of the environmental disturbance torques. Therefore, the estimates of the vehicle's angular momentum include errors due to gyro measurement errors and uncertainty in the dynamic model. The relationship between the true angular momentum vector, $\vec{h}$, and the estimated angular momentum vector, $\hat{\vec{h}}$, is

$$\delta\bar{h}^b(t) = \bar{h}^b(t) - \hat{\bar{h}}^b(t) \tag{29}$$

where $\delta\vec{h}$ refers to the estimation error of the angular momentum vector.

The differential equation for the angular momentum estimation error can be derived by differentiating Eq. (29)

$$\delta\dot{\bar{h}}^b = \dot{\bar{h}}^b - \dot{\hat{\bar{h}}}^b \tag{30}$$

The attitude dynamic equations for the true and estimated angular momentum can be written using Eq. (28)

$$\dot{\bar{h}}^b = -\bar{\omega}^{b\times}\bar{h}^b + \bar{G}^b_{ext} = -\bar{\omega}^{b\times}(\hat{\bar{h}}^b + \delta\bar{h}^b) + \bar{G}^b_{ext} \tag{31a}$$

$$\dot{\hat{\bar{h}}}^b = -\hat{\bar{\omega}}^{b\times}\hat{\bar{h}}^b + \hat{\bar{G}}^b_{ext} \tag{31b}$$

where Eq. (29) has been substituted into Eq. (31a). $\hat{\vec{G}}_{ext}$ refers to estimated external torque vector acting on the vehicle. If Eq. (31) is substituted into Eq. (29), then $\delta\dot{\vec{h}}$ can be written as

$$\begin{aligned}\delta\dot{\bar{h}}^b &= -\bar{\omega}^{b\times}(\hat{\bar{h}}^b + \delta\bar{h}^b) + \bar{G}^b_{ext} - (-\hat{\bar{\omega}}^{b\times}\hat{\bar{h}}^b + \hat{\bar{G}}^b_{ext}) \\ &= -\bar{\omega}^{b\times}\delta\bar{h}^b - (\bar{\omega}^b - \hat{\bar{\omega}}^b)^\times\hat{\bar{h}}^b + \bar{\mathrm{G}}^b_{ext} - \hat{\bar{G}}^b_{ext}\end{aligned} \tag{32}$$

If Eqs. (11) and (26) are substituted into Eq. (32), then $\delta\dot{\vec{h}}$ can be rewritten as

$$\begin{aligned}\delta\dot{\bar{h}}^b &= -(\hat{\bar{\omega}}^b - C_{b\,g}[\delta\bar{b}^g + \bar{n}^g_g])^\times\delta\bar{h}^b - (I^{-1}\delta\bar{h}^b + I^{-1}\delta I\hat{\bar{\omega}}^b)^\times\hat{\bar{h}}^b + \bar{G}^b_{ext} - \hat{\bar{G}}^b_{ext} \\ &= -(\hat{\bar{\omega}}^{b\times} - \hat{\bar{h}}^{b\times}I^{-1})\delta\bar{h}^b - \delta\bar{h}^{b\times}C_{b\,g}\delta\bar{b}^g - \delta\bar{h}^{b\times}C_{b\,g}\bar{n}^g_g - (I^{-1}\delta I\hat{\bar{\omega}}^b)^\times\hat{\bar{h}}^b + \delta\bar{G}^b_{ext}\end{aligned} \tag{33}$$

where the second order terms are assumed to be very small. $\delta\vec{G}_{ext}$ refers to the error of the external torque vector

$$\delta\bar{G}^b_{ext} = \bar{G}^b_{ext} - \hat{\bar{G}}^b_{ext} \tag{34}$$

It should be noted that $\delta\vec{G}_{ext}$ depends on the application and orbit parameters.

F. State Vector Equations

The equations used to formulate and propagate the state mean vectors for both IA VMA architectures are

$$\dot{\hat{\bar{h}}}^b(t) = -\hat{\bar{\omega}}^{b\times}(t)\hat{\bar{h}}^b(t) + \hat{\bar{G}}^b_{ext}(t) \tag{31b}$$

$$\dot{\hat{q}}(t) = \frac{1}{2}\Omega[\hat{\bar{\omega}}^b(t)]\hat{q}(t) \tag{21b}$$

$$\dot{\hat{\bar{b}}}^g(t) = \bar{0} \tag{12}$$

where

$$\hat{\bar{\omega}}^b(t) = C_{b\,g}\bar{\omega}^g_m(t) - C_{b\,g}\hat{\bar{b}}^g(t) \tag{8}$$

The dynamic model for the first IA VMA architecture includes the attitude kinematic equations, the gyro measurement model, and the gyro bias model. The state vector corresponding to this model has seven states consisting of four quaternion states and three gyro bias states. The dynamic model for the second IA VMA architecture includes the attitude dynamic equations, the attitude kinematic equations, the gyro measurement model, and the gyro bias model. The state vector corresponding to this model has ten states consisting of three angular momentum states, four quaternion states, and three gyro bias states.

The attitude kinematic equations provide a geometric relationship between a vehicle's attitude rates and angular velocity. Therefore, these equations are not constrained by the vehicle's inertia and resulting dynamics. The attitude dynamic equations are included in the dynamic model of the second IA VMA architecture to constrain the attitude kinematic equations by forcing the attitude kinematics to match the measurements of angular velocity. As a result, the second IA VMA architecture should exhibit improved performance as compared to the first IA VMA architecture at a specific gyro grade or in the event of aiding system sensor unavailability or failure.

G. State Error Covariance Equations

The equations used to formulate and propagate the state error covariance matrices for both IA VMA architectures are based on the following state error vector equations

$$\begin{aligned}
\delta\dot{\bar{h}}^{b}(t) &= -(\hat{\bar{\omega}}^{b\times}(t) - \hat{\dot{\bar{h}}}^{b\times}(t)I^{-1})\delta\bar{h}^{b}(t) - \delta\bar{h}^{b\times}(t)C_{b\,g}\delta\bar{b}^{g}(t) - \delta\bar{h}^{b\times}(t)C_{b\,g}\bar{n}_{g}^{g}(t) \\
&\quad - (I^{-1}\delta I\hat{\bar{\omega}}^{b}(t))^{\times}\hat{\bar{h}}^{b}(t) + \delta\bar{G}_{ext}^{b}(t) \qquad (33) \\
\delta\dot{\bar{q}}(t) &= -\hat{\bar{\omega}}^{b\times}(t)\delta\bar{q}(t) - \frac{1}{2}C_{b\,g}\delta\bar{b}^{g}(t) - \frac{1}{2}C_{b\,g}\bar{n}_{g}^{g}(t) + \frac{1}{2}\delta\bar{q}^{\times}(t)I^{-1}\delta\bar{h}^{b}(t) - \frac{1}{2}(I^{-1}\delta I\hat{\bar{\omega}}^{b}(t))^{\times}\delta\bar{q}(t) \qquad (27) \\
&= -\hat{\bar{\omega}}^{b\times}(t)\delta\bar{q}(t) - \frac{1}{2}C_{b\,g}\delta\bar{b}^{g}(t) - \frac{1}{2}C_{b\,g}\bar{n}_{g}^{g}(t) \qquad (24) \\
\delta\dot{\bar{b}}^{g}(t) &= -\frac{1}{\tau}\delta\bar{b}^{g}(t) + \bar{n}_{b}^{g}(t) \qquad (13)
\end{aligned}$$

The state error vector corresponding to the dynamic model of the first IA VMA architecture has six states consisting of three quaternion estimation error states and three gyro bias error states

$$\delta\bar{x}_{1}(t) = [\,\delta\bar{q}^{T}(t) \quad \delta\bar{b}^{gT}(t)\,]^{T} \qquad (35)$$

In matrix form, the state error vector equations are

$$\frac{d}{dt}\delta\bar{x}_{1} = \begin{bmatrix} -\hat{\bar{\omega}}^{b\times} & -(1/2)C_{b\,g} \\ \bar{0}_{3\times3} & -(1/\tau)\bar{1}_{3} \end{bmatrix}\delta\bar{x}_{1} + \begin{bmatrix} -(1/2)C_{b\,g} & \bar{0}_{3\times3} \\ \bar{0}_{3\times3} & \bar{1}_{3} \end{bmatrix}\begin{bmatrix} \bar{n}_{g}^{g} \\ \bar{n}_{b}^{g} \end{bmatrix} \qquad (36)$$

where Eq. (24) has been used to rewrite $\delta\dot{\bar{q}}$.

The state error vector corresponding to the dynamic model of the second IA VMA architecture has nine states consisting of three angular momentum estimation error states, three quaternion estimation error states, and three bias error states

$$\delta\bar{x}_{2}(t) = [\,\delta\bar{h}^{bT}(t) \quad \delta\bar{q}^{T}(t) \quad \delta\bar{b}^{gT}(t)\,]^{T} \qquad (37)$$

In matrix form, the state error vector equations are

$$\frac{d}{dt}\delta\bar{x}_{2} = \begin{bmatrix} F_{2,11} & \bar{0}_{3\times3} & -\delta\bar{h}^{b\times}C_{b\,g} \\ (1/2)\delta\bar{q}^{\times}(t)I^{-1} & F_{2,22} & -(1/2)C_{b\,g} \\ \bar{0}_{3\times3} & \bar{0}_{3\times3} & -(1/\tau)\bar{1}_{3} \end{bmatrix}\delta\bar{x}_{2} + \begin{bmatrix} \bar{1}_{3} & -\delta\bar{h}^{b\times}C_{b\,g} & \bar{0}_{3\times3} \\ \bar{0}_{3\times3} & -(1/2)C_{b\,g} & \bar{0}_{3\times3} \\ \bar{0}_{3\times3} & \bar{0}_{3\times3} & \bar{1}_{3} \end{bmatrix}\begin{bmatrix} \delta\bar{G}_{ext}^{b} \\ \bar{n}_{g}^{g} \\ \bar{n}_{b}^{g} \end{bmatrix} \qquad (38)$$

$$\begin{aligned}
F_{2,11} &= -(\hat{\bar{\omega}}^{b\times}(t) - \hat{\dot{\bar{h}}}^{b\times}(t)I^{-1}) \\
F_{2,22} &= -\hat{\bar{\omega}}^{b\times} + (1/2)(I^{-1}\delta I\hat{\bar{\omega}}^{b}(t))^{\times}
\end{aligned}$$

where Eq. (27) has been used to rewrite $\delta\dot{\bar{q}}$.

The state covariance equations for the dynamic models of both IA VMA architectures can be derived from the (linearized) state error vector equations. The general form of the continuous-time state error vector equations is

$$\frac{d}{dt}\delta\bar{x}(t) = F(t)\delta\bar{x}(t) + \Gamma_{c}(t)\bar{w}(t) \qquad (39)$$

where F refers to the $n \times n$ continuous-time state error mapping matrix, Γ_{c} refers to the $n \times m$ continuous-time process noise mapping matrix, and $\vec{w}$ refers to the $m \times 1$ process noise vector.

The general form of the discrete-time state error vector equations can be determined by solving Eq. (39)

$$\delta\bar{x}_{k+1} = \exp[F_k(t_{k+1} - t_k)]\delta\bar{x}_k + \int_{t_k}^{t_{k+1}} \exp[F(\tau)]\Gamma_c(\tau)\bar{w}(\tau)\, d\tau \tag{40}$$

If Γ_c and $\vec{w}$ are assumed constant throughout the time interval (t_k, t_{k+1}), then Eq. (40) can be rewritten as

$$\delta\bar{x}_{k+1} = \Phi_k\delta\bar{x}_k + \Gamma_k\bar{w}_k \tag{41a}$$

where

$$\Phi_k = \exp[F_k(t_{k+1} - t_k)] \tag{41b}$$

$$\Gamma_k = \int_{t_k}^{t_{k+1}} \exp[F(\tau)]\, d\tau\Gamma_c(t_k) \tag{41c}$$

The discrete-time state covariance matrix equations corresponding to both IA VMA architectures are

$$P_{1,k+1/k} = \Phi_{1,k}P_{1,k/k}\Phi_{1,k}^T + Q_{1,k} \tag{42a}$$

$$P_{2,k+1/k} = \Phi_{2,k}P_{2,k/k}\Phi_{2,k}^T + Q_{2,k} \tag{42b}$$

where at time t_k, Q_k refers to the discrete-time equivalent of $\Gamma_c(t)Q_W(t)\Gamma_c^T(t)$ and is assumed to be constant throughout the time interval (t_k, t_{k+1})

$$Q_k = \int_{t_k}^{t_{k+1}} \Phi\left(t_{k+1}, \tau\right)\Gamma_c(\tau)Q_W(\tau)\Gamma_c^T(\tau)\Phi^T\left(t_{k+1}, \tau\right)\, d\tau \tag{43}$$

where Q_W refers to the power spectral density matrix of the process noise vector

$$Q_{W1}(t) = \text{diag}\left[\sigma_{gx}^2,\, \sigma_{gy}^2,\, \sigma_{gz}^2,\, \frac{2\sigma_{b1x}^2}{\tau_x},\, \frac{2\sigma_{b1y}^2}{\tau_y},\, \frac{2\sigma_{b1z}^2}{\tau_z}\right] \tag{44a}$$

$$Q_{W2}(t) = \text{diag}\left[\delta G_x^{b2},\, \delta G_y^{b2},\, \delta G_z^{b2},\, \sigma_{gx}^2,\, \sigma_{gy}^2,\, \sigma_{gz}^2,\, \tfrac{2\sigma_{b1x}^2}{\tau_z},\, \tfrac{2\sigma_{b1y}^2}{\tau_y},\, \tfrac{2\sigma_{b1z}^2}{\tau_z}\right] \tag{44b}$$

The state error covariance matrix can be interpreted as follows. $\delta\vec{h}$ refers to the angular momentum estimation errors and, thus, the corresponding entries of the estimated covariance matrix are the variances of the probability density function (pdf) of the angular momentum estimation errors. $\delta\bar{q}$ refers to the quaternion estimation errors and, thus, the corresponding entries of the estimated covariance matrix are the variances of the pdf of the quaternion estimation errors. $\delta\vec{b}$ refers to the gyro bias errors and, thus, the corresponding entries of the estimated covariance matrix are the variances of the pdf of the gyro bias estimation errors. Therefore, the corresponding entries of the estimated state error covariance matrix are the variances of the pdf of the state error vector and not of the pdf of the estimated state vector itself.

Tuning parameters can be incorporated into Γ_c to adjust the uncertainty of the dynamic models and to smooth the estimates computed by the filter

$$\Gamma_{c1} = \begin{bmatrix} -(1/2)\alpha_1 C_{b\,g} & \bar{0}_{3\times3} \\ \bar{0}_{3\times3} & \beta_1\bar{1}_3 \end{bmatrix} \tag{45a}$$

$$\Gamma_{c2} = \begin{bmatrix} \gamma_2\bar{1}_3 & -\kappa_2\delta\bar{h}^{b\times}C_{b\,g} & \bar{0}_{3\times3} \\ \bar{0}_{3\times3} & -(1/2)\alpha_2 C_{b\,g} & \bar{0}_{3\times3} \\ \bar{0}_{3\times3} & \bar{0}_{3\times3} & \beta_2\bar{1}_3 \end{bmatrix} \tag{45b}$$

where α_1, β_1, α_2, β_2, γ_2, and κ_2 refer to tuning parameters.

In general, the process noise is used to incorporate uncertainty into the dynamic models of the stochastic system. For the IA VMA architectures, this uncertainty includes the gyro biases, gyro measurement models, the vehicle's inertia, applied control torques, and models of the external disturbance torques. There is a trade-off when adjusting these tuning parameters because they control the location of the closed loop estimator poles. In general, as the tuning parameters are increased, the estimator poles become faster, the estimator gains increase,

and the filter convergence time decreases. However, the estimates computed by the filter become noisier. As the tuning parameters are decreased, the estimator poles become slower, the estimator gain decreases, and the filter convergence time increases. However, the estimates computed by the filter become smoother. It should be noted that these generalized statements do not automatically apply to linearized stochastic systems or for coupled state error vector equations.

III. Measurement Model

A nonlinear measurement model must be linearized for application with the update equations of the Kalman filter, to compute the Kalman gain matrix, and to compute estimates of the statistics of the state vector. The linearized measurement model can be derived by considering an arbitrary vector $\vec{u}$ of the set of vectors $\mathcal{U} = [\vec{u}_1, ..., \vec{u}_n]$ and the reference frames $\mathcal{F}_N$ and $\mathcal{F}_b$. The relationship between the representation of $\vec{u}$ as resolved in the frames $\mathcal{F}_N$ and $\mathcal{F}_b$ is

$$\bar{u}^b_m(t) = C_{b\,N}(q)\bar{u}^N(t) \tag{46}$$

where $\vec{u}$ is considered to be measured in $\mathcal{F}_b$, $\bar{u}^b_m$, and modeled in $\mathcal{F}_N$, $\bar{u}^N$, without loss of generality. If the sensor frame is not aligned with $\mathcal{F}_b$, then the scalar components of the measured vector are assumed to be transformed to $\mathcal{F}_b$ using the appropriate DCM.

The EKFs implemented for the IA VMA architectures compute estimates of the true quaternions using measurements from the gyros and aiding sensors, the models of the vehicle's attitude motion, and the sensor measurement models. The quaternion estimation errors are due to sensor errors such as bias and wide band noise, sensor misalignment, uncertainty in the vehicle's dynamic models and sensor measurement models, vehicle position errors, and filter computational errors. These sources cause three types of estimation errors:

1) origin of the estimated navigation and body frames
2) direction of the Euler axis of rotation, $\hat{e}$
3) magnitude of the rotation, Φ, about $\hat{e}$

Therefore, the EKFs use an estimated navigation frame, $\mathcal{F}_{\hat{N}}$, to generate the modeled vectors. Furthermore, the DCM, parameterized by the estimated quaternion, specifies the orientation of an estimated body frame, $\mathcal{F}_{\hat{b}}$, to $\mathcal{F}_{\hat{N}}$. The relationships between the true and estimated quaternions and their corresponding DCMs can be written as

$$q(t) = \delta q_b(t) \otimes \hat{q}(t) \otimes \delta q_N(t) \tag{47a}$$

$$C_{b\,N} = C_{b\,\hat{b}}(\delta q_b) C_{\hat{b}\,\hat{N}}(\hat{q}) C_{\hat{N}\,N}(\delta q_N) \tag{47b}$$

where $C_{\hat{b}\,\hat{N}}$ refers to the DCM from $\mathcal{F}_{\hat{N}}$ to $\mathcal{F}_{\hat{b}}$ parameterized using the estimated quaternion $\hat{q}$, $C_{b\,\hat{b}}$ refers to the DCM from $\mathcal{F}_{\hat{b}}$ to $\mathcal{F}_b$ parameterized using the quaternion error δq_b, and $C_{\hat{N}\,N}$ refers to the DCM from $\mathcal{F}_N$ to $\mathcal{F}_{\hat{N}}$ parameterized using the quaternion error δq_N. Equation (47) suggests that the rotation from the navigation frame to the body frame is equal to the rotation from the navigation frame to the estimated navigation frame followed by a rotation from the estimated navigation frame to the estimated body frame followed by a rotation from the estimated body frame to the body frame.

The linearized measurement model is derived using the following assumptions:

1) the vehicle's position errors are small
2) the quaternion estimation errors can be lumped into either δq_N or δq_b
3) the quaternion errors δq_N and δq_b refer to small angles

The source of the vehicle's position errors is its navigation system. These position errors are, effectively, the positions errors of the origin of $\mathcal{F}_{\hat{N}}$ and $\mathcal{F}_{\hat{b}}$ relative to the origin of $\mathcal{F}_N$ and $\mathcal{F}_b$. Therefore, the position errors force the EKF into using modeled vectors with incorrect magnitude and direction. However, if the vehicle's position errors are small and the modeled vectors are insensitive to small position errors, then the errors of the modeled vectors can be considered negligible or a component of δq_N or δq_b.

The application of these three assumptions enables the true quaternion to be written using two quaternion error models. The first model can be written as

$$q(t) = \hat{q}(t) \otimes \delta q_N(t) \tag{48a}$$

$$C_{b\,N} = C_{b\,\hat{N}} C_{\hat{N}\,N} = C_{b\,\hat{N}}[\bar{1}_3 - 2\delta\bar{q}^{\times}_N] \tag{48b}$$

Equation (48) suggests that the rotation from $\mathcal{F}_N$ to $\mathcal{F}_b$ is equal to the rotation from $\mathcal{F}_N$ to $\mathcal{F}_{\hat{N}}$ followed by a rotation from $\mathcal{F}_{\hat{N}}$ to $\mathcal{F}_{\hat{b}}$. The second model, Fig. 2, can be written as

$$q(t) = \delta q_b(t) \otimes \hat{q}(t) \tag{49a}$$
$$C_{b\,N} = C_{b\,\hat{b}} C_{\hat{b}\,N} = [\bar{1}_3 - 2\delta\bar{q}_b^{\times}] C_{\hat{b}\,N} \tag{49b}$$

Equation (49) suggests that the rotation from $\mathcal{F}_N$ to $\mathcal{F}_b$ is equal to the rotation from $\mathcal{F}_N$ to $\mathcal{F}_{\hat{b}}$ followed by a rotation from $\mathcal{F}_{\hat{b}}$ to $\mathcal{F}_{\hat{b}}$. This second model corresponds to the relationship between q and $\hat{q}$ as defined in Eq. (20).

Two linearized measurement models can be derived for the first quaternion error model. For the first measurement model, if Eq. (48b) is substituted into Eq. (46), then $\bar{u}_m^b$ can be written as

$$\bar{u}_m^b = C_{b\,\hat{N}} [\bar{1}_3 - 2\delta\bar{q}_N^{\times}] \bar{u}^N \tag{50}$$

If Eq. (50) is multiplied by $C_{\hat{N}\,b}$, then

$$\begin{aligned} C_{\hat{N}\,b} \bar{u}_m^b &= [\bar{1}_3 - 2\delta\bar{q}_N^{\times}] \bar{u}^N \\ \delta\bar{z}^N &= -2\bar{u}^{N\times} \delta\bar{q}_N \end{aligned} \tag{51}$$

where $\delta\bar{z}^N = \bar{u}^N - \bar{u}_m^{\hat{N}}$ and refers to the measurement error vector. Since this derivation was performed for an arbitrary $\vec{u}$ of $\mathcal{U}$, the same derivation is valid for all $\vec{u}_i \in \mathcal{U}$ and, thus, Eq. (51) can be rewritten as

$$\begin{bmatrix} \delta\bar{z}_1^N \\ \vdots \\ \delta\bar{z}_n^N \end{bmatrix} = \begin{bmatrix} -2\bar{u}_1^{N\times} \\ \vdots \\ -2\bar{u}_n^{N\times} \end{bmatrix} \delta\bar{q}_N = H_{N1} \delta\bar{q}_N \tag{52}$$

where H_{N1} refers to the measurement matrix and is formulated using the modeled vectors.

For the second measurement model, if the transpose of Eq. (48b) is substituted into the transpose of Eq. (46), then $\bar{u}_N$ can be written as

$$\begin{aligned} \bar{u}^N &= [\bar{1}_3 + 2\delta\bar{q}_N^{\times}] C_{\hat{N}\,b} \bar{u}_m^b \\ \delta\bar{z}^N &= -2\bar{u}_m^{\hat{N}\times} \delta\bar{q}_N \end{aligned} \tag{53}$$

Therefore, for all $\vec{u}_i \in \mathcal{U}$, Eq. (53) can be rewritten as

$$\begin{bmatrix} \delta\bar{z}_1^N \\ \vdots \\ \delta\bar{z}_n^N \end{bmatrix} = \begin{bmatrix} -2\bar{u}_{1m}^{\hat{N}\times} \\ \vdots \\ -2\bar{u}_{nm}^{\hat{N}\times} \end{bmatrix} \delta\bar{q}_N = \begin{bmatrix} -2(C_{\hat{N}\,b}\bar{u}_{1m}^b)^{\times} \\ \vdots \\ -2(C_{\hat{N}\,b}\bar{u}_{nm}^b)^{\times} \end{bmatrix} \delta\bar{q}_N = H_{N2} \delta\bar{q}_N \tag{54}$$

where H_{N2} refers to the measurement matrix and is formulated using the estimated quaternions and the measured vectors.

Two linearized measurement models can be derived for the second quaternion error model. For the first measurement model, if Eq. (49b) is substituted into Eq. (46), then $\bar{u}_m^b$ can be written as

$$\begin{aligned} \bar{u}_m^b &= [\bar{1}_3 - 2\delta\bar{q}_b^{\times}] C_{\hat{b}\,N} \bar{u}^N \\ \delta\bar{z}^b &= -2\bar{u}^{\hat{b}\times} \delta\bar{q}_b \end{aligned} \tag{55}$$

where $\delta\bar{z}^b = \bar{u}^{\hat{b}} - \bar{u}_m^b$. Therefore, for all $\vec{u}_i \in \mathcal{U}$, Eq. (55) can be rewritten as

$$\begin{bmatrix} \delta\bar{z}_1^b \\ \vdots \\ \delta\bar{z}_n^b \end{bmatrix} = \begin{bmatrix} -2\bar{u}_1^{\hat{b}\times} \\ \vdots \\ -2\bar{u}_n^{\hat{b}\times} \end{bmatrix} \delta\bar{q}_b = \begin{bmatrix} -2(C_{\hat{b}\,N}\bar{u}_1^N)^{\times} \\ \vdots \\ -2(C_{\hat{b}\,N}\bar{u}_n^N)^{\times} \end{bmatrix} \delta\bar{q}_b = H_{b1} \delta\bar{q}_b \tag{56}$$

where H_{b1} refers to the measurement matrix and is formulated using the estimated quaternions and the modeled vectors.

For the second measurement model, if the transpose of Eq. (49b) is substituted into the transpose of Eq. (46), then $\bar{u}_N$ can be written as

$$\bar{u}^N = C_{\hat{N}\,b}[\bar{1}_3 + 2\delta\bar{q}_b^{\times}]\bar{u}_m^b \tag{57}$$

If Eq. (57) is multiplied by $C_{\hat{b}\,N}$, then

$$\begin{aligned} C_{\hat{b}\,N}\bar{u}^N &= [\bar{1}_3 + 2\delta\bar{q}_b^{\times}]\bar{u}_m^b \\ \delta\bar{z}^b &= -2\bar{u}_m^{b\times}\delta\bar{q}_b \end{aligned} \tag{58}$$

Therefore, for all $\vec{u}_i \in \mathcal{U}$, Eq. (58) can be rewritten as

$$\begin{bmatrix} \delta\bar{z}_1^b \\ \vdots \\ \delta\bar{z}_n^b \end{bmatrix} = \begin{bmatrix} -2\bar{u}_{1m}^{b\times} \\ \vdots \\ -2\bar{u}_{nm}^{b\times} \end{bmatrix} \delta\bar{q}_b = H_{b2}\delta\bar{q}_b \tag{59}$$

where H_{b2} refers to the measurement matrix and is formulated using the measured vectors.

Four linearized measurement matrices have been derived for the two quaternion error models. The linearized measurement matrix selected for the filter should be formulated from the vectors with the smallest uncertainty. Therefore, H is formulated using the modeled vectors rather than the measured vectors. If the first quaternion error model is used, then H_{N1} should be selected for the EKF. If the second quaternion error model is used, then H_{b1} should be selected for the EKF.

Equations (52), (54), (56), and (59) show why Wahba's problem requires measurements of at least two non-zero, non-collinear vectors to compute a unique DCM. A skew-symmetric matrix is singular and, thus, the skew-symmetric matrices in these equations can not be inverted to determine $\delta\bar{q}$. Physically, a singularity of the skew-symmetric matrix indicates that there is a rotational ambiguity in the direction of the vector used to formulate the matrix. Therefore, the second vector is used to remove this rotational ambiguity.

It must be noted that the direction of $\hat{e}$ is fixed for a small angle rotation. The small angle assumption was applied to derive the linearized measurement model and applies only during the measurement update. The estimates of $\hat{e}$ and Φ can change during the time update where the small angle assumption does not apply. Only the estimates of Φ can change during the measurement update where the small angle assumption does apply.

The implementation of the VMA to compute real-time estimates of a vehicle's attitude requires the following information

1) at least one non-zero set of vector measurements in $\mathcal{F}_b$
2) models of the vector measurement in $\mathcal{F}_N$ stored on board the vehicle
3) the time of the vector measurements
4) the position of the vehicle

The vector measurements are typically made using TAMs, star trackers, and Sun sensors. The models for the Earth's magnetic field vector and the star and Sun positions relative to the vehicle require the position of the vehicle. Furthermore, the models for the star and Sun positions require the time of the measurement to account for the Earth's orbit about the Sun.

IV. Filter Algorithm

The general design of the EKF for both IA VMA architectures is shown in Fig. 3. During the time update, the gyro measurements are used to propagate both dynamic models. Therefore, the estimated state mean vector and state error covariance matrix are propagated at the gyro sampling frequency. The gyro measurements are used to increase the bandwidth of the aiding sensor estimates of the vehicle's attitude, to smooth attitude estimates in between aiding sensor measurements, and to provide attitude measurements in the event of aiding sensor unavailability or failure. The gyro measurements are corrected using the posterior estimate of the mean gyro bias before these measurements are used to perform the time update.

During the measurement update, the estimates of the state mean vector and state error covariance matrix are corrected at the aiding sensor sampling frequency. The linear Kalman filter equations are used with the linearized measurement matrix and corresponding measurement error vector. It should be noted that the posterior estimates of the quaternion mean are normalized to preserve the quaternion unit constraint.

The EKF [18], [19] for both IA VMA architectures can be described as follows

Initialization

$$\hat{\bar{h}}_0^b = E\{\bar{h}_0^b\} \tag{60}$$
$$\hat{q}_0 = E\{q_0\} \tag{61}$$
$$\hat{\bar{b}}_0^g = E\{\bar{b}_0^g\} \tag{62}$$
$$P_0 = E\{\delta\bar{x}_0 \delta\bar{x}_0^T\} \tag{63}$$

Time Update

$$\hat{\bar{\omega}}_{k/k}^b = C_{b\,g}\bar{\omega}_{m,k}^g - C_{b\,g}\hat{\bar{b}}_{k/k}^g \tag{64}$$
$$\hat{\bar{h}}_{k+1/k}^b = f(\hat{\bar{\omega}}_{k/k}^b, \hat{\bar{h}}_{k/k}^b, \hat{\bar{G}}_{ext,k}^b) \tag{65}$$
$$\hat{q}_{k+1/k} = \exp\left(\frac{1}{2}\Omega \begin{bmatrix} \hat{\bar{\omega}}_{k/k}^b \\ 0 \end{bmatrix} (t_{k+1} - t_k)\right) \hat{q}_{k/k} \tag{66}$$
$$\hat{\bar{b}}_{k+1/k}^g = \hat{\bar{b}}_{k/k}^g \tag{67}$$
$$P_{k+1/k} = \Phi_k P_{k/k} \Phi_k^T + Q_k \tag{68}$$

Measurement Update

$$K_{k+1} = P_{k+1/k} H_{k+1}^T (R_{k+1} + H_{k+1} P_{k+1/k} H_{k+1}^T)^{-1} \tag{69}$$
$$P_{k+1/k+1} = (\bar{1} - K_{k+1} H_{k+1}) P_{k+1/k} \tag{70}$$
$$\delta\bar{x}_{k+1} = K_{k+1}\delta\bar{z}_{k+1} \tag{71}$$
$$\hat{\bar{h}}_{k+1/k+1}^b = \hat{\bar{h}}_{k+1/k}^b + \delta\bar{h}_{k+1} \tag{72}$$
$$\hat{q}_{k+1/k+1} = \delta q_{k+1} \otimes \hat{q}_{k+1/k} = \begin{bmatrix} \delta\hat{\bar{q}}_{k+1} \\ 1 \end{bmatrix} \otimes \hat{q}_{k+1/k} \tag{73}$$
$$\hat{\bar{b}}_{k+1/k+1}^g = \hat{\bar{b}}_{k+1/k}^g + \delta\bar{b}_{k+1} \tag{74}$$
$$\hat{q}_{k+1/k+1} = \frac{\hat{q}_{k+1/k+1}}{||\hat{q}_{k+1/k+1}||} \tag{75}$$

where

$$H_{1,k+1} = \begin{bmatrix} -2(C_{\hat{b}\,N}(\hat{q}_{1,k+1/k})\bar{u}_{1,k+1}^N)^\times & \bar{0}_{3\times3} \\ \vdots & \vdots \\ -2(C_{\hat{b}\,N}(\hat{q}_{1,k+1/k})\bar{u}_{n,k+1}^N)^\times & \bar{0}_{3\times3} \end{bmatrix} \tag{76}$$
$$\delta\bar{z}_{1,k+1} = \begin{bmatrix} C_{\hat{b}\,N}(\hat{q}_{1,k+1/k})\bar{u}_{1,k+1}^N - \bar{u}_{1m,k+1}^b \\ \vdots \\ C_{\hat{b}\,N}(\hat{q}_{1,k+1/k})\bar{u}_{n,k+1}^N - \bar{u}_{nm,k+1}^b \end{bmatrix} \tag{77}$$
$$H_{2,k+1} = \begin{bmatrix} \bar{0}_{3\times3} & -2(C_{\hat{b}\,N}(\hat{q}_{2,k+1/k})\bar{u}_{1,k+1}^N)^\times & \bar{0}_{3\times3} \\ \vdots & \vdots & \vdots \\ \bar{0}_{3\times3} & -2(C_{\hat{b}\,N}(\hat{q}_{2,k+1/k})\bar{u}_{n,k+1}^N)^\times & \bar{0}_{3\times3} \end{bmatrix} \tag{78}$$
$$\delta\bar{z}_{2,k+1} = \begin{bmatrix} C_{\hat{b}\,N}(\hat{q}_{2,k+1/k})\bar{u}_{1,k+1}^N - \bar{u}_{1m,k+1}^b \\ \vdots \\ C_{\hat{b}\,N}(\hat{q}_{2,k+1/k})\bar{u}_{n,k+1}^N - \bar{u}_{nm,k+1}^b \end{bmatrix} \tag{79}$$

V. Application of the IA VMA Architectures

The objective of the following simulations is to evaluate the performance of the EKFs implemented for both IA VMA architectures by conducting trade studies using the gyro grade as the varying parameter. The performance of the EKFs implemented for both architectures was evaluated using post-processed data measured on the Stanford Gravity Probe (GP-B) spacecraft. The calibration of spaceflight data, the simulation of gyro measurements corresponding to various gyro grades, and the simulation of the EKFs using the calibrated and simulated data were performed using Matlab.

A. Gravity Probe B Spacecraft

The GP-B spacecraft [20], [21] was an on-orbit experiment designed and constructed by Stanford University, NASA, and Lockheed Martin to investigate several predictions resulting from Einstein's general theory of relativity. In April 2004, the GP-B spacecraft was inserted into a polar orbit with a semi-major axis of $7027.4\,km$, an eccentricity of 0.0014, and an orbital period of $97.7\,min$. The GP-B spacecraft is a prolate shaped body, spin stabilized about its minor axis with a nominal spin rate of $0.7742\,rpm$ $(4.65^\circ/s)$. This minor, or spin, axis pointed to the guide star IM Pegasi (HR 8703). IM Pegasi had a right ascension angle of 343.26° and a declination angle of 16.84° during the time of the experiment. The spacecraft used thrusters to maintain a drag free orbit. Furthermore, the spacecraft used a combination of thrusters and magnetic torquers to maintain its spin rate with no nutation angle. Therefore, the spacecraft's angular momentum vector was, effectively, fixed relative to inertial space.

The GP-B spacecraft was equipped with a sensor set that included gyros aligned with the spacecraft's spin axis, a TAM, two star trackers, and GPS sensors. The gyros were specifically designed for this experiment and had a maximum drift rate of $10^{-11\circ}/hr$. The gyros had a sampling frequency of $1\,Hz$. The TAM was located on a boom to minimize interference with other components onboard the spacecraft. The TAM's measurement axes were nominally aligned with the principal axes of the spacecraft. The TAM had wide band noise with standard deviation $< 10\,mV$ (rms) on each axis and a sampling frequency of $0.1\,Hz$.

B. Reference Frames

The VMA requires two reference frames for operation: a body frame and a navigation frame. For this application, the GP-B body frame, $\mathcal{F}_b$, is assumed to be the principal axis frame of the spacecraft with origin located at the spacecraft's center of mass. The body Z axis is aligned with the spin axis of the spacecraft. The GP-B navigation frame, $\mathcal{F}_N$, is assumed to be an inertial frame that shares a common origin with the GP-B body frame. The navigation Z axis points to the guide star and is coincident with the body Z axis. The navigation X axis points in the most northerly direction relative to the Earth center inertial (ECI) frame. The three axes of the GP-B body frame are coincident with the axes of the GP-B navigation frame when the spin angle of the spacecraft is zero.

The DCM between the ECI frame and the GP-B navigation frame can be parameterized using a 3-2-3 Euler angle sequence. The first Euler angle refers to a rotation about the ECI Z axis through the right ascension angle of the guide star. The second Euler angle rotation refers to a rotation about the intermediate Y axis through 90° minus the declination angle of the guide star. The Z axis of this second intermediate frame points to the guide star and is aligned with the GP-B navigation Z axis. The third Euler angle refers to a rotation about the second intermediate Z axis through 180°. The DCM between the GP-B navigation frame and the GP-B body frame can be parameterized using an Euler angle rotation about the navigation Z axis through the spin angle of the spacecraft.

C. Measurement Data Processing

To evaluate the EKF's performance, the gyro measurements for the GP-B spacecraft's spin axis were corrupted with correlated and uncorrelated noise components using the gyro measurement model defined in Eq. (3). Since the spacecraft had no angular velocity about its body X and Y axes, the gyro measurements for these two axes were simulated using the model defined in Eq. (3) at the same sampling frequency and times of the spin axis gyro. The gyro measurements were corrupted or simulated using the statistics given in Table 1, regardless of gyro grade or IA VMA architecture. The standard deviation of the gyro bias drift rate, σ_{b1}, depends on the gyro grade. The selection of numerical values for the gyro bias will be discussed shortly.

The TAM measurements were calibrated using a batch least squares formulation based on the following measurement model [22]

$$\bar{m}^b_{m,k}(t) = C_{MC}\bar{m}^b_k(t) + \bar{b}^b_m + \bar{n}^b_{m,k}(t) \tag{80a}$$

$$C_{MC} = C_m C_{sf} C_{si} \tag{80b}$$

where at time t_k, $\vec{m}_m$ refers to the local EMF measurement vector, $\vec{m}$ refers to a the model of the EMF vector, C_{MC} refers to a 3×3 calibration matrix, C_m refers to a 3×3 misalignment error matrix, C_{sf} refers to a 3×3 scale factor error matrix, C_{si} refers to a 3×3 soft iron error matrix, $\vec{b}_m$ refers to a hard iron bias error vector, and $\vec{n}_m$ refers to a wide band TAM measurement noise vector. C_m is the misalignment error of the measurement axes of the TAM relative relative to the GP-B body frame. We assume that the misalignment error is small and write C_m using a small angle assumption. The vector $\vec{m}$ was generated from the IGRF-95 EMF model [23] using the GPS sensor position measurements of the GP-B spacecraft.

The twelve calibration parameters corresponding to the TAM measurement model are given in Table 2. Fig. 4 shows the calibrated TAM measurements for approximately one and a half orbits. Fig. 4 indicates that the TAM measured four local maxima or minima along its Z measurement axis and four local maxima or minima along its X and Y measurement axes during one orbit. The TAM Z measurement axis was aligned with the local EMF vector between $35^\circ - 50^\circ$ N latitude and $40^\circ - 50^\circ$ S latitude. The TAM measurement Z axis was orthogonal to the local EMF vector at polar and equatorial latitudes. The magnitude of the local maximum and minimum TAM measurements along its X and Y measurement axes were greater at the polar latitudes as compared to the equatorial latitudes. The spacecraft crossed the North pole at approximately $1160\,s$ and $7020\,s$ and crossed the South pole at approximately $4090\,s$ and $9940\,s$. The spacecraft crossed the equator at approximately $2622\,s$, $5556\,s$, and $8482\,s$.

D. EKF Performance

The EKFs for both IA VMA architectures were simulated using the algorithm outlined in Section IV. The system matrices for both architectures were selected as follows. The matrix Q_W was defined in Eq. (44) and numerical values were given in Table 1. The attitude control torques applied to the GP-B spacecraft were selected, in part, to reject the effect of disturbance torques acting on the spacecraft. The maximum magnitude of the control torques applied to the spacecraft was $0.01\,Nm$ and, thus, $\delta\bar{G}^b$ was set equal to $0.01\,Nm$ in each axis. The tuning parameters for the process noise mapping matrices were set equal to one: $\alpha_1, \beta_1, \alpha_2, \beta_2, \gamma_2, \kappa_2 = 1$. The measurement noise covariance matrix was selected to be diagonal with the square of the TAM wide band noise rms values in the diagonal elements. These rms values were converted to Tesla (T) using the scale factors for each TAM measurement axis.

The statistics of the initial state vector were selected as follows. The initial mean quaternion was selected randomly using the Matlab's random number generator. It was not limited or constrained within a certain angle of the spacecraft's true initial attitude. The initial mean gyro null shifts were selected randomly using Matlab's random number generator. These initial estimates of the state mean vector were selected to be the same for both IA VMA architectures. The initial mean angular momentum vector was set equal to the spacecraft's true initial angular momentum vector for all simulations. The initial state error covariance matrices were selected as

$$P_{10} = \text{diag}\,[0.1,\, 0.1,\, 0.1,\, 2^\circ/s,\, 2^\circ/s,\, 2^\circ/s] \tag{81a}$$

$$P_{20} = \text{diag}\left[2\,kgm^2/s,\, 2\,kgm^2/s,\, 2\,kgm^2/s,\, 0.1,\, 0.1,\, 0.1,\, 2^\circ/s,\, 2^\circ/s,\, 2^\circ/s\right] \tag{81b}$$

EKF simulations were performed for both architectures using standard deviations of the gyro bias drift rate of $18^\circ/hr$ and $180^\circ/hr$. This range of gyro bias drift rates is representative of tactical or consumer grade rate gyros, respectively. The time update rate for all simulations was at the gyro sampling frequency of $1\,Hz$. The measurement update rate for all simulations was at the TAM sampling frequency of $0.1\,Hz$. Figures 5-16 show the average of 100 Monte Carlo simulations of the EKF performance for the second IA VMA architecture using all three gyro grades for approximately one and a half GP-B spacecraft orbits. Figures for the EKF performance for the first IA VMA architecture have not been included for reasons described shortly. It should be noted that the linearized state error mapping matrix and the measurement matrices for both EKF architectures were confirmed to be observable in the sense that the observability grammian [AM], [STE]

$$\mathcal{O}_N^T \mathcal{O}_N = \sum_{k=1}^{N} \Phi_{k-1,0}^T H_k^T H_k \Phi_{k-1,0} \tag{82}$$

had full rank following a finite number of TAM measurements, N. At time t_k, $\mathcal{O}_k$ refers to the $kp \times n$ observability matrix, $\Phi_{k-1,0} = \Phi_{k-1} \cdots \Phi_0$, and $\Phi_{k-1,0}^T = \Phi_0^T \cdots \Phi_{k-1}^T$.

Figures 5-10 show the EKF performance for a standard deviation of the gyro bias drift rate of $18^\circ/hr$ or $0.005^\circ/s$. Figures 11-16 show the EKF performance for a standard deviation of the gyro bias drift rate of $180^\circ/hr$ or $0.05^\circ/s$. In Figures 6, 8, 10, 12, 14, and 16, the state error vector is represented by solid lines whereas the $1-\sigma$ estimation error bands are represented by dashed lines. The estimated mean angular velocity vector shown in these figures was computed directly from the estimated mean angular momentum vector. The estimated Euler angles were computed directly from the estimated mean quaternions.

Figures 5, 7, and 9 show the estimated means of the angular velocity vector, Euler angles, and gyro null shifts. Figures 6, 8, and 10 show the error vectors and the $1-\sigma$ estimation error bands for the angular momentum vector, quaternions, and gyro null shifts. These figures show that the estimates of the state mean vector converged within half of a GP-B spacecraft orbit using the IA VMA architecture with a gyro grade of $18^\circ/hr$. Furthermore, the estimates of the state mean vector converged regardless of the initial estimates of the quaternions and gyro null shifts.

The estimates of the mean bias null shifts converged to within $\pm 0.02^\circ/s$ within $2000\,s$ of EKF initialization and show the effect of both correlated and uncorrelated gyro bias components. The $1-\sigma$ estimation error bands of the gyro null shifts are of the same order of magnitude as the standard deviation of the gyro bias drift rate in each axis.

The estimates of the mean roll and pitch angles are generally within $\pm 2^\circ$ of the true GP-B spacecraft roll and pitch angles. However, as the spacecraft passes through latitudes ranging from $40^\circ - 50^\circ$ and approaches either polar or equatorial latitudes, the yaw and pitch angle errors increase to $\pm 4^\circ$ because the local EMF vector is aligned with the TAM Z measurement axis. The estimate of the mean spin angle has a bias of approximately 1° and the spin angle error is generally within $\pm 1^\circ$ of this bias value. However, as the spacecraft passes through polar latitudes, the bias of the estimated mean spin angle increases to approximately 2° and the spin angle errors are generally within $\pm 2^\circ$ of this bias value because the local EMF vector is orthogonal to the TAM Z measurement axis. The $1-\sigma$ estimation error bands of the quaternion error vector were less than ± 0.015 in the X and Y body axes and less than ± 0.02 in the Z body axis satisfying the small angle characterization involved with the design of the measurement matrix.

The estimates of the mean angular velocity vector converged within $1000\,s$ of EKF initialization. Since the estimated mean roll and pitch rates were $\pm 0.7^\circ/s$, the spin rate of the spacecraft was underestimated by $1.2^\circ/s$. The norm of the estimated mean angular velocity vector was $4.3^\circ/s$ corresponding to a bias error of $0.35^\circ/s$. The $1-\sigma$ estimation error bands of the angular momentum vector remained at $2\,kgm^2/s$ in each axis.

Figures 11, 13, and 15 show the estimated means of the angular velocity vector, Euler angles, and gyro null shifts. Figures 12, 14, and 16 show the error vectors and the $1-\sigma$ estimation error bands for the angular momentum vector, quaternions, and gyro null shifts. These figures show that the estimates of the state mean vector converged within half of a GP-B spacecraft orbit using the IA VMA architecture with a gyro grade of $180^\circ/hr$. Furthermore, the estimates of the state mean vector converged regardless of the initial estimates of the quaternions and gyro null shifts. However, the magnitude of the estimation errors for this gyro grade were consistently larger than for a gyro grade of $18^\circ/hr$.

The estimates of the mean bias null shifts converged to within $\pm 0.15^\circ/s$ within $2000\,s$ of EKF initialization and show the effect of both correlated and uncorrelated gyro bias components. The $1-\sigma$ estimation error bands of the gyro null shifts are of the same order of magnitude as the standard deviation of the gyro bias drift rate in each axis.

The estimates of the mean roll and pitch angles are generally within $\pm 2.5^\circ$ of the true GP-B spacecraft roll and pitch angles. However, as the spacecraft passes through latitudes ranging from $40^\circ - 50^\circ$ and approaches either polar or equatorial latitudes, the yaw and pitch angle axes errors increase to $\pm 5^\circ$ because the local EMF vector is aligned with the TAM Z measurement axis. The estimate of the mean spin angle has a bias of approximately 2° and the spin angle error is generally within $\pm 2.5^\circ$ of this bias value. However, as the spacecraft passes through polar latitudes, the spin angle axis errors increase to $\pm 12^\circ$ of this bias value because the local EMF vector is orthogonal to the TAM Z measurement axis. The $1-\sigma$ estimation error bands of the quaternion error vector were less than ± 0.02 in the X and Y body axes and less than ± 0.05 in the Z body axis satisfying the small angle characterization involved with the design of the measurement matrix.

The estimates of the mean angular velocity vector converged within $500\,s$ of EKF initialization. Since the estimated mean roll and pitch rates were $\pm 1.1^\circ/s$, the spin rate of the spacecraft was underestimated by $1.8^\circ/s$. The norm of the estimated mean angular velocity vector was $3.97^\circ/s$ corresponding to a bias error of $0.67^\circ/s$. The $1-\sigma$ estimation error bands of the angular momentum vector remained at $2\,kgm^2/s$ in each axis.

Several general observations can be made regarding the performance of the EKFs implemented for the IA

VMA architectures. First, the EKFs of both architectures computed estimates of the state vector statistics that were nearly identical at both gyro grades. The objective of comparing the EKF performance of both architectures at each gyro grade was to determine whether mathematically constraining the vehicle's attitude motion would result in smaller magnitude of both the bias errors of the estimated state mean vector and the $1-\sigma$ estimation error bands of the state vector. However, because the GP-B spacecraft's angular momentum vector was, effectively, fixed relative to inertial space, the spacecraft's angular motion was already constrained before the sensor measurements were taken. Therefore, there was little effect in including the attitude dynamic equations in the IA VMA architecture. A comparison of EKF performance for both architectures at a specific gyro grade requires sensor measurements from a spacecraft performing three-axis attitude maneuvers. For these reasons, we show only the EKF performance for the second IA VMA architecture.

Second, the estimates of the state vector statistics suggest that the GP-B spacecraft is undergoing nutational motion. The period of this nutation motion is $77.4\,s$ which corresponds to the spin rate of the spacecraft. The error sources of both IA VMA architectures include the statistics of the initial state vector, uncertainty in the attitude dynamic equations and gyro measurement model which feeds back into the other elements of the state vector, errors of the calibrated TAM measurements, and linearization of the nonlinear dynamic and measurements models. The errors resulting from these sources, especially the sensor model and measurement errors, feed back into the dynamic model of both architectures and resulted in the estimated nutation angle of the spacecraft's angular velocity vector about the true angular momentum vector. This estimated nutational motion is seen throughout Figures 5-16. As the the gyro grade decreases, the magnitude of the estimated nutational motion increases.

Third, the $1-\sigma$ estimation error bands of both the quaternion error vector and the gyro bias null shifts depend on both the orbital position and attitude of the GP-B spacecraft. It is the orientation of the spacecraft relative to the local EMF vector that governs the magnitude of the EMF measurements along the TAM measurement axes. The spacecraft's orbital motion, spacecraft's orientation, and varying magnitude of the local EMF vector are reflected in the periodically varying magnitude of the $1-\sigma$ estimation error bands plots. It can be seen that as the magnitude of the local EMF vector increases along the TAM Z measurement axis, the magnitude of the $1-\sigma$ estimation error bands decreases in the spacecraft body Z axis and increases in the spacecraft body X and Y axes. Furthermore, as the magnitude of the local EMF vector increases along along the TAM X and Y measurement axes, the magnitude of the $1-\sigma$ estimation error bands increases in the spacecraft body Z axis and decreases in the spacecraft body X and Y axes.

Fourth, the EKFs of both architectures computed estimates of the state vector statistics that depend on the gyro grade. More specifically, the magnitude of the $1-\sigma$ estimation error bands of the gyro null shifts had the same order of magnitude as the standard deviation of the gyro bias drift rate and the errors of the estimated mean gyro bias null shifts increased to the actual values of the gyro null shifts. The errors of the estimated mean gyro bias null shifts feed back into the other elements of the state vector. If the EKF is unable to estimate the gyro bias null shift, then the aiding sensor provided insufficient information to reset the gyro based estimates of the spacecraft's attitude. However, there is a gyro grade for the EKFs implemented for the IA VMA architectures that can be used to estimate a spacecraft's attitude. These results suggest that if the standard deviation of the gyro bias drift rate is less than or equal to $180^\circ/hr$, then a gyro and TAM can be used as the only two sensors of an AD system for a spin stabilized spacecraft. The AD or pointing requirements of the spacecraft dictate the actual quality of the gyro to be used with this AD system.

VI. Conclusion

In this paper, we have designed an AD system for a spin stabilized spacecraft using a sensor set consisting of rate gyros and a TAM, two IA VMA architectures, and an EKF to blend the sensor measurements and compute estimates of the spacecraft's attitude. The VMA is a filtering algorithm that numerically solves Wahba's problem by linearizing the DCM between the spacecraft's body and navigation frames. The measurement matrix for both IA VMA architectures is designed using the VMA. The VMA is then extended using two dynamic models. The first model includes the spacecraft's attitude kinematic equations and a gyro measurement model. The second model includes the spacecraft's attitude dynamic and kinematic equations, and a gyro measurement model.

We conducted trade studies to evaluate the EKF performance for both IA VMA architectures as a function of the gyro grade using post-processed spaceflight data measured on the Stanford GP-B spacecraft. Several conclusions can be drawn from the analysis of the trade studies.

First, the trade studies showed that gyro grades with standard deviation of bias drift rate less than or equal to $180^\circ/hr$ can be used in spacecraft AD systems and provide attitude estimates with errors of the estimated mean attitude less than $\pm 12^\circ$. Furthermore, the trade studies showed that gyro grades with standard deviation of bias

drift rate less than or equal to $18°/hr$ can be used in spacecraft AD systems and provide attitude estimates with errors of the estimated mean attitude less than $\pm 4°$.

Second, the trade studies confirm the feasibility of using this sensor set for spacecraft AD systems with limited AD or pointing requirements. The spacecraft attitude is unobservable at one epoch using a vector measurement from a TAM. However, the direction of the local EMF vector varied relative to the GP-B spacecraft as it orbited the Earth. Therefore, the direction of the vector measurements from the TAM varied over a series of epochs and the spacecraft attitude was observable using a series of vector measurements from a TAM over these epochs. The potentially unbounded errors in the gyro based estimates of the spacecraft's attitude can be bounded using vector measurements from a TAM.

Acknowledgments

This work was partially supported by NASA under Minnesota Space Grant NNG05GG39H.

References

[1] V.L. Bageshwar, D. Gebre-Egziabher, William L. Garrard, et al, "Minnesat: GPS Attitude Determination Experiments Onboard a Nanosatellite," 20^{th} AIAA/Utah State University Conference on Small Satellites, Logan Utah, August 2006, SSC06-VII-7.

[2] G. Wahba, "A Least Squares Estimate of Satellite Attitude, Problem 65-1," *Siam Review*, Vol. 7, No. 3, July 1965, pp. 409.

[3] H.D. Black, "A Passive System for Determining the Attitude of a Satellite," *AIAA Journal*, Vol. 2, No. 7, 1964, pp. 1350-1351.

[4] G. Wahba, "A Least Squares Estimate of Satellite Attitude, Solution," *Siam Review*, Vol. 8, No. 3, July 1966, pp. 384-386.

[5] M.D. Shuster and S.D. Oh, "Three-Axis Determination from Vector Observations," *AIAA Journal of Guidance, Control, and Dynamics*, Vol. 4, No. 1, Jan.-Feb. 1981, pp. 70-77.

[6] I.Y. Bar-Itzhack, "REQUEST: A Recursive QUEST Algorithm for Sequential Attitude Determination," *AIAA Journal of Guidance, Control, and Dynamics*, Vol. 19, No. 5, Sept.-Oct. 1996, pp. 1034-1038.

[7] I.Y. Bar-Itzhack and M. Idan, "Recursive Attitude Determination from Vector Observations: Euler angle estimation," *AIAA Journal of Guidance, Control, and Dynamics*, Vol. 10, No. 2, 1987, pp. 152-157.

[8] I.Y. Bar-Itzhack and J. Reiner, "Recursive Attitude Determination from Vector Observations: Direction Cosine Matrix Identification," *AIAA Journal of Guidance, Control*, and *Dynamics*, Vol. 7, No. 1, 1984, pp. 51-56.

[9] M. Idan, "Estimation of Rodrigues Parameters from Vector Observations," *IEEE Transactions on Aerospace Electronic Systems*, Vol. 32, No. 2, 1996, pp. 578-585.

[10] I.Y. Bar-Itzhack and Y. Oshman, "Attitude Determination from Vector Observations: Quaternion Estimation," *IEEE Transactions on Aerospace Electronic Systems*, Vol. 21, No. 1, 1985, pp. 128-136.

[11] D. Choukroun, I.Y. Bar-Itzhack, and Y. Oshman, "Novel Quaternion Kalman Filter," *IEEE Transactions on Aerospace and Electronic Systems*, Vol. 42, No. 1, Jan. 2006, pp. 174-190.

[12] M.L. Psiaki, "Attitude-Determination Filtering via Extended Quaternion Estimation," *AIAA Journal of Guidance, Control, and Dynamics*, Vol. 23, No. 2, March-April 2000, pp. 206-214.

[13] D. Gebre-Egziabher, G.H. Elkaim, J.D. Powell, and B.W. Parkinson, "A Gyro-Free, Quaternion Based Attitude Determination System Suitable for Implementation Using Low-Cost Sensors," in *Proceedings of the IEEE Position, Location, and Navigation Symposium*, PLANS 2000, pp. 185-192.

[14] D. Gebre-Egziabher, R.C. Hayward, and J.D. Powell, "Design of Multi-Sensor Attitude Determination Systems," *IEEE Transactions on Aerospace and Electronic Systems*, Vol. 40, No. 2, April 2004, pp. 627-649.

[15] J.B. Kuipers, *Quaternions and Rotation Sequences*. Princeton, New Jersey: Princeton University Press, 2002.

[16] G. Creamer, "Spacecraft Attitude Determination using Gyros and Quaternion Measurements," *Journal of Astronautical Sciences*, Vol. 44, No. 3, July-Sept. 1996, pp. 357-371.

[17] P.C. Hughes, *Spacecraft Attitude Dynamics*. New York: John Wiley & Sons, 1986.

[18] B.D.O. Anderson and J.B. Moore, *Optimal Filtering*. Mineola, NY: Dover Publications, Inc. 1995.

[19] R.F. Stengel, *Optimal Control and Estimation*. Mineola, NY: Dover Publications, Inc., 1994.

[20] "Gravity Probe B: Launch Companion," http://einstein.stanford.edu and http:// www.gravityprobeb.com.

[21] "Gravity Probe B: Testing Einstein's Universe," NASA Fact Sheet FS-2005-01-05-MSFC, Pub 8-4039, http://www.nasa.gov, http://einstein.stanford.edu, and http:// www.gravityprobeb.com.

[22] D. Gebre-Egziabher, G.H. Elkaim, J.D. Powell, and B.W. Parkinson, "Calibration of Strapdown Magnetometers in Magnetic Field Domain," *ASCE Journal of Aerospace Engineering*, Vol. 19, No. 2, April 2006, pp. 87-102.

[23] C.E. Barton, "International Geomagnetic Reference Field: the Seventh Generation," *Journal of Geomagnetism and Geoelectricity*, Vol. 49, No. 2, 1997, pp. 123-148.

	Grade 1	Grade 2
b_{0x}	0.9°/*s*	0.9°/*s*
b_{0y}	1.0°/*s*	1.0°/*s*
b_{0z}	1.1°/*s*	1.1°/*s*
τ_x,τ_y,τ_z	300 *s*	300 *s*
$\sigma_{gx},\sigma_{gy},\sigma_{gz}$	0.05°/*s*	0.05°/*s*
$\sigma_{b1x},\sigma_{b1y},\sigma_{b1z}$	18°/*hr*	180°/*hr*

Table 1. Rate Gyro Bias Statistics

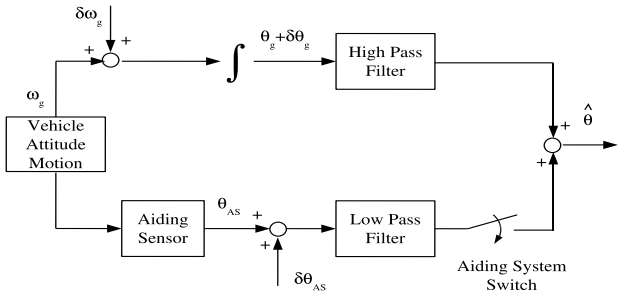

Figure 1. Complementary/Kalman Filter

$C_{MC}(1,1)$	-0.500
$C_{MC}(1,2)$	0.369
$C_{MC}(1,3)$	0.817
$C_{MC}(2,1)$	-0.562
$C_{MC}(2,2)$	-0.809
$C_{MC}(2,3)$	-0.00343
$C_{MC}(3,1)$	0.646
$C_{MC}(3,2)$	-0.440
$C_{MC}(3,3)$	0.616
$\bar{b}_m(1)$	-0.105
$\bar{b}_m(2)$	-0.135
$\bar{b}_m(3)$	-0.145

Table 2. TAM Calibration Parameters

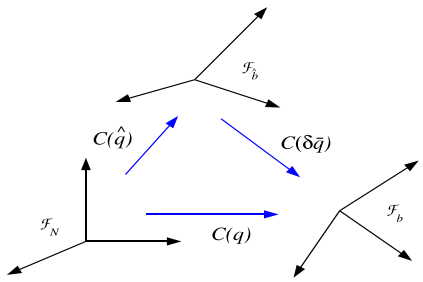

Figure 2. VMA Reference Frames

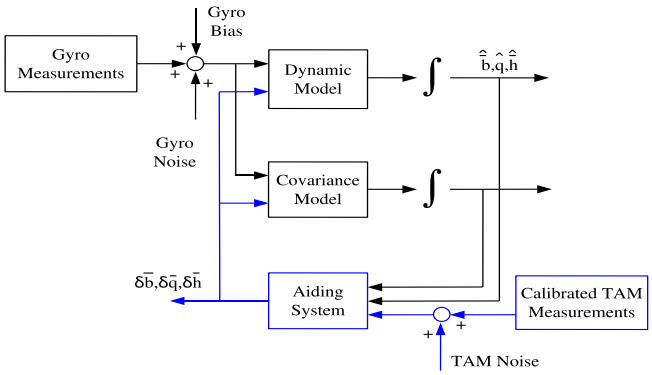

Figure 3. IA VMA Architecture

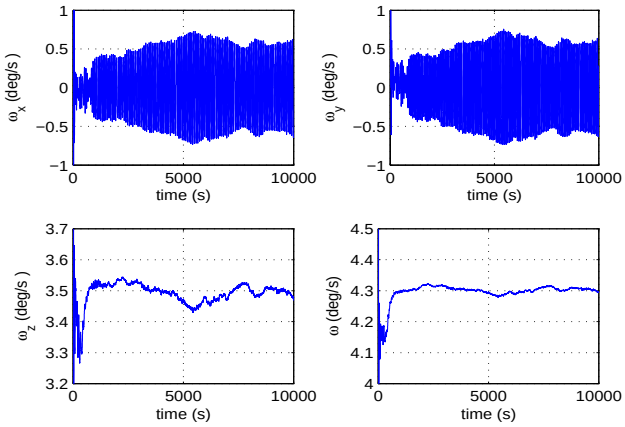

Figure 5. Estimated GP-B Spacecraft Mean Angular Velocity Vector; Standard Deviation, Gyro Bias Drift Rate: $18°/hr$

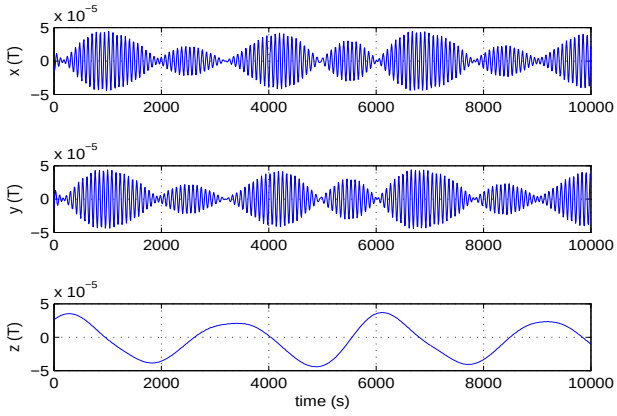

Figure 4. Calibrated TAM Measurements

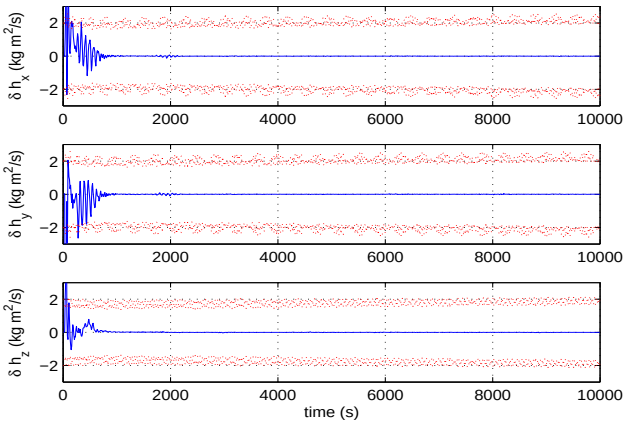

Figure 6. $1-\sigma$ **Estimation Error Bands of Angular Momentum Vector; Standard Deviation, Gyro Bias Drift Rate:** $18°/hr$

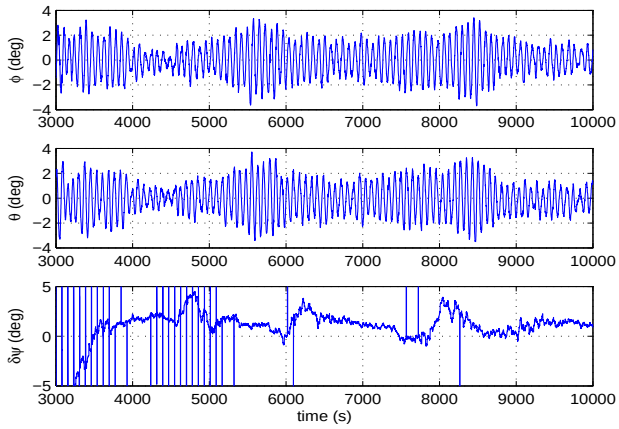

Figure 7. Estimated GP-B Spacecraft Mean Euler Angles; Standard Deviation, Gyro Bias Drift Rate: $18°/hr$

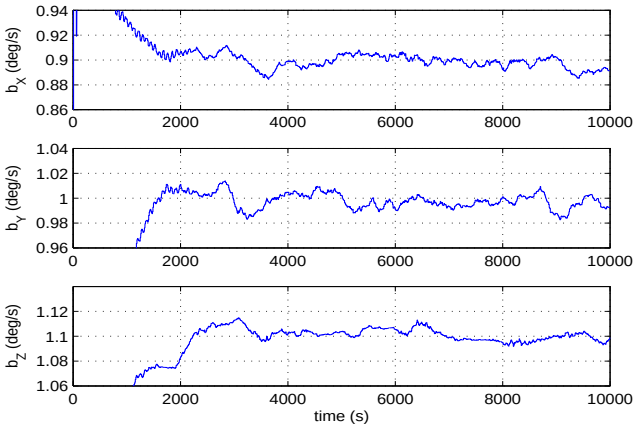

Figure 9. Estimated Mean Gyro Bias Null Shifts; Standard Deviation, Gyro Bias Drift Rate: $18°/hr$

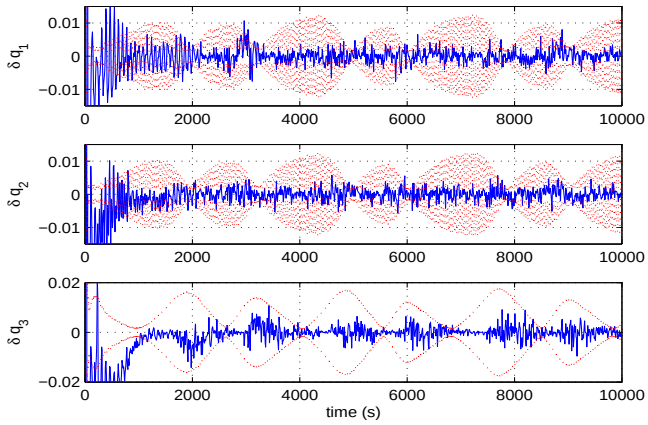

Figure 8. $1-\sigma$ **Estimation Error Bands of Quaternion Estimation Error; Standard Deviation, Gyro Bias Drift Rate:** $18°/hr$

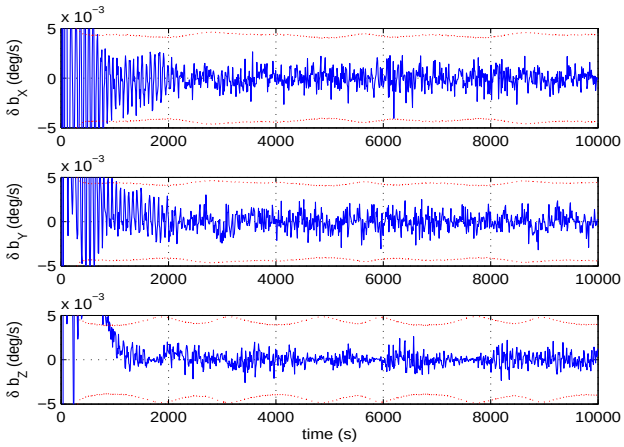

Figure 10. $1-\sigma$ **Estimation Error Bands of Gyro Bias Null Shifts; Standard Deviation, Gyro Bias Drift Rate:** $18°/hr$

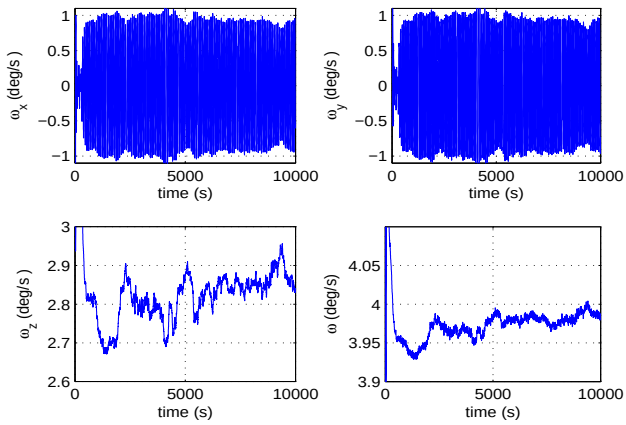

Figure 11. Estimated GP-B Spacecraft Mean Angular Velocity Vector; Standard Deviation, Gyro Bias Drift Rate: $180°/hr$

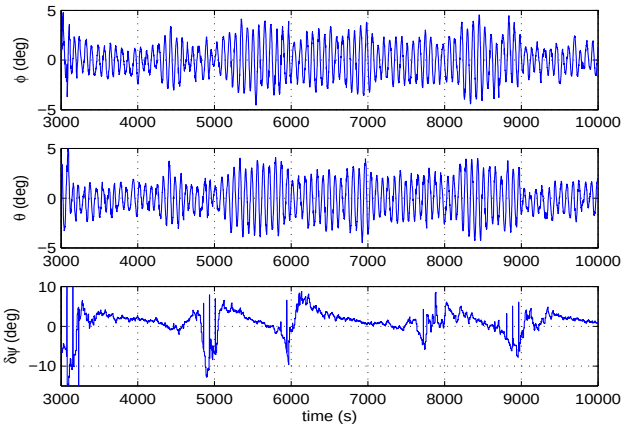

Figure 13. Estimated GP-B Spacecraft Mean Euler Angles; Standard Deviation, Gyro Bias Drift Rate: $180°/hr$

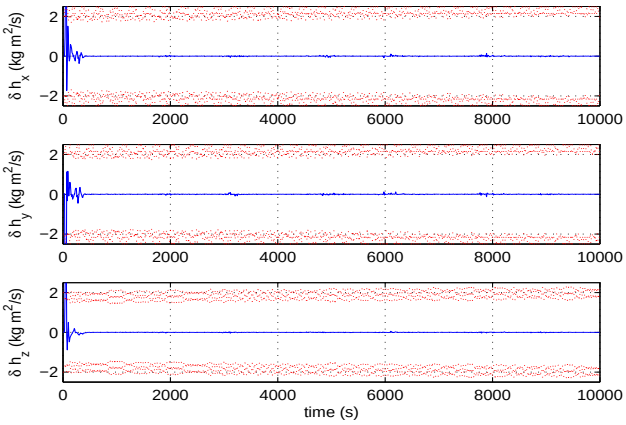

Figure 12. $1-\sigma$ **Estimation Error Bands of Angular Momentum Vector; Standard Deviation, Gyro Bias Drift Rate:** $180°/hr$

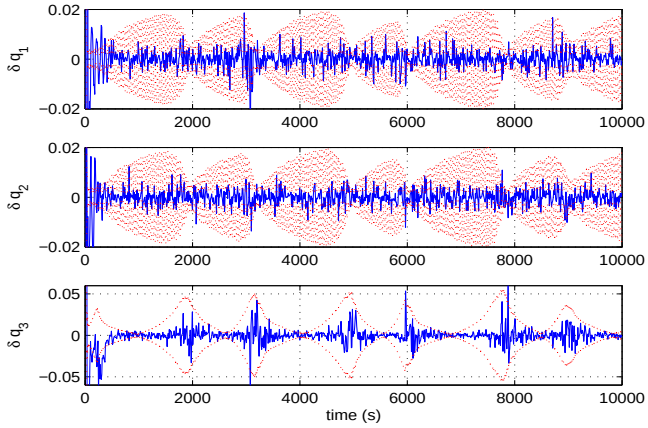

Figure 14. $1-\sigma$ **Estimation Error Bands of Quaternion Estimation Error; Standard Deviation, Gyro Bias Drift Rate:** $180°/hr$

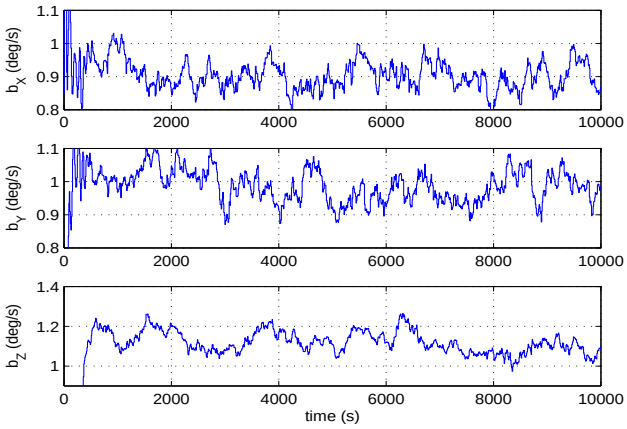

Figure 15. Estimated Mean Gyro Bias Null Shifts; Standard Deviation, Gyro Bias Drift Rate: $180^\circ/hr$

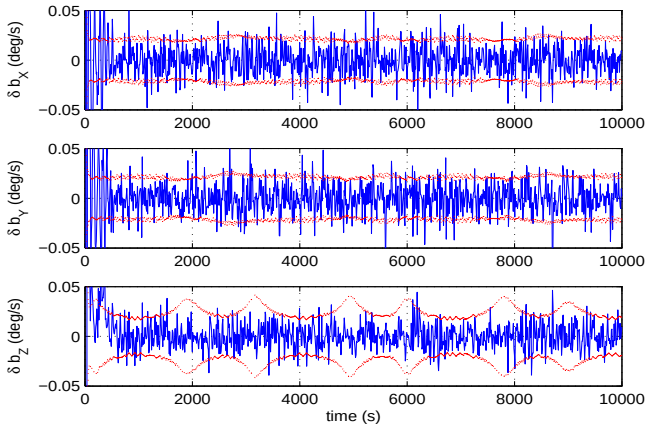

Figure 16. $1-\sigma$ **Estimation Error Bands of Gyro Bias Null Shifts; Standard Deviation, Gyro Bias Drift Rate:** $180^\circ/hr$